Design and Fabrication of Physiologic Tissue Scaffolds
Using Projection-Micro-Stereolithography

by

Micha Sam Brickman Raredon

B.S., Yale University (2011)

Submitted to the Department of Materials Science and Engineering
in Partial Fulfillment of the Requirements for the Degree of

Master of Science

at the

MASSACHUSETTS INSTITUTE OF TECHNOLOGY

June 2014

Signature of Author: Signature redacted
Micha Sam Brickman Raredon
May 23, 2014

Certified by: Signature redacted
Jeffrey Borenstein
Director of Biomedical Research, Draper Laboratories
Thesis Supervisor

Certified by: Signature redacted
Linda Griffith
S.E.T.I. Professor of Biological and Mechanical Engineering
Director, MIT Center for Gynepathology Research
Thesis Supervisor

Certified by: Signature redacted
Paula Hammond
David H. Koch Professor in Engineering, Department of Chemical Engineering
Thesis Supervisor

Certified by: Signature redacted
Darrell Irvine
Professor of Materials Science and Engineering and Biological Engineering
Thesis Reader

Accepted by: Signature redacted
Gerbrand Ceder
R.P. Simmons Professor of Materials Science and Engineering
Chair, Departmental Committee on Graduate Students

Design and Fabrication of Physiologic Tissue Scaffolds
Using Projection-Micro-Stereolithography

by

Micha Sam Brickman Raredon

Submitted to the Department of Materials Science and Engineering on May 23, 2014
in Partial Fulfillment of the Requirements for the Degree of Master of Science in
Materials Science and Engineering

ABSTRACT

Recent advances in material processing are presenting groundbreaking opportunities for biomedical engineers. Projection-micro-stereolithography, or PuSL, is an additive manufacturing technique in which complex parts are built out of UV-curable resins using ultraviolet light. The primary strength of PuSL is its capacity to translate CAD files into three-dimensional parts with unusually small feature sizes (~0.5 microns). It is an ideal candidate, therefore, for making tissue scaffolds with sophisticated microscopic architecture.

Nearly all multicellular biological tissues display a hierarchy of scale. In human tissues, this means that the mechanics and function of an organ are defined by structural organization on multiple levels. Macroscopically, a branching blood supply creates a patent network for nutrient delivery and gas exchange. Microscopically, these vessels spread into capillary beds shaped in an organ-specific orientation and organization, helping to define the functional unit of a given tissue. On a nano-scale, the walls of these capillaries have a tissue-specific structure that selectively mediates the diffusion of nutrients and proteins. To craft a histologically accurate tissue, each of these length scales must be considered and mimicked in a space-filling fashion.

In this project, I sought to generate acellular, degradable tissue scaffolds that mimicked native extracellular matrix across length scales. The research described here lays the groundwork for the generation of degradable, vascularized cell scaffolds that might be used to build architecturally complex multi-cellular tissues suitable for both pharmacological modeling and regenerative medicine.

Thesis Supervisors:

Jeffrey Borenstein
Director of Biomedical Research, Draper Laboratories

Linda Griffith
S.E.T.I. Professor of Biological and Mechanical Engineering
Director, MIT Center for Gynepathology Research

Paula Hammond
David H. Koch Professor in Engineering, Department of Chemical Engineering

Table of Contents

Introduction and project outline

i.0 Overview

A fundamental aim of this research was to fabricate structures that look like the vascular bed of a liver with the cells removed, and to develop a methodology for visualizing and drawing such structures. Without cells, the basement membrane of a vascular network appears as a suspended network of nano-porous hollow tubes, with empty space both inside, in the lumen of the capillaries, and outside, between each micro-vessel. Although there have been many attempts to generate vascularized tissues, some of which have been reasonably successful, most have sought to generate solid constructs out of gels or cell suspensions. This research is unusual in that it aimed to build the basement membrane of a vascular network without luminal or parenchymal cells, the idea being that these could be seeded later.

There were three parts to achieving this aim:

1) Build a fabrication apparatus to allow the construction of such scaffolds
2) Engineer a resin mixture that would allow the fabrication of these scaffolds with the proper nanostructure
3) Develop protocols and CAD designs to yield functional scaffolds

i.1 Background

This work was done in association with the DARPA- and NIH-funded BIO-MIMETICS initiative, a project to create a small-scale in vitro analogue of the human body with 10-12 interacting tissue types connected via an artificial circulatory system, often colloquially referred to as a "human body on a chip." The aim of this project is to create a bench-top platform with interchangeable tissue modules, each of which contains a piece of organ-specific living tissue.

Ideally, this system will model chemical and biological interactions between liver, lung, gut, cardiac, neural, and other relevant tissue types, with each organ module communicating with the others via micro-fluidic media circulation.

Such platforms have high potential to impact pharmacological development. It is common for drug candidates to show initial promise and then fail when brought into animal models or even to clinical trials. These failures occur because drug candidates that seem promising when tested on isolated tissue types in the laboratory can yield toxic byproducts when metabolized or modified by the different tissue types in the body. Since organ-specific interactions are hard to predict, it is desirable that an in vitro model be made to allow multiple-organ-system testing of drugs without animal or clinical trials.[1-3]

The success of this endeavor relies on the ability to generate robust tissues in the laboratory that closely resemble native tissues both in terms of function and chemical response. As is often the case in biology, the functions of various tissue types are intimately dependent on their form. However, for many years biological engineers have lacked the proper tools to build tissues that display a histological architecture comparable to that found in vivo. This thesis has been an active collaboration among the laboratories of Linda Griffith, Paula Hammond, Jeffrey Borenstein, and Nick Fang, in an attempt to harness recent advances in materials processing to develop technology and techniques that might allow ultra-high resolution fabrication of three-dimensional acellular tissue scaffolds with biomimetic micro-architecture.

Consequently, this research also has relevant implications for regenerative medicine. The ability to create scaffolds with functional microvasculature, patterned in organ-specific fashions, might open a pathway to commercial fabrication of complex, large-scale tissues suitable for in vivo implantation. Although there are many additional hurdles that would need to be overcome

for this long-term vision to be a reality, the work described here presents a promising avenue toward scalable synthetic fabrication of vascularized acellular scaffolds, which for multiple decades has been an overbearing obstacle for the field of regenerative medicine.[4-8]

i.2 Existing liver platform

During previous years, the Griffith lab has developed a robust small-scale bioreactor capable of generating and maintaining 8mm diameter liver tissue analogues in vitro, and this design has acted as a technologic platform for expanding to multiple tissue types in the BIO-MIMETICS program. Much of the work presented here has been carried out with this design architecture in mind. Figure i.1 shows the device, first published in 2010, and commercially developed by Zyoxel (now CN Bio Innovations Limited).[9]

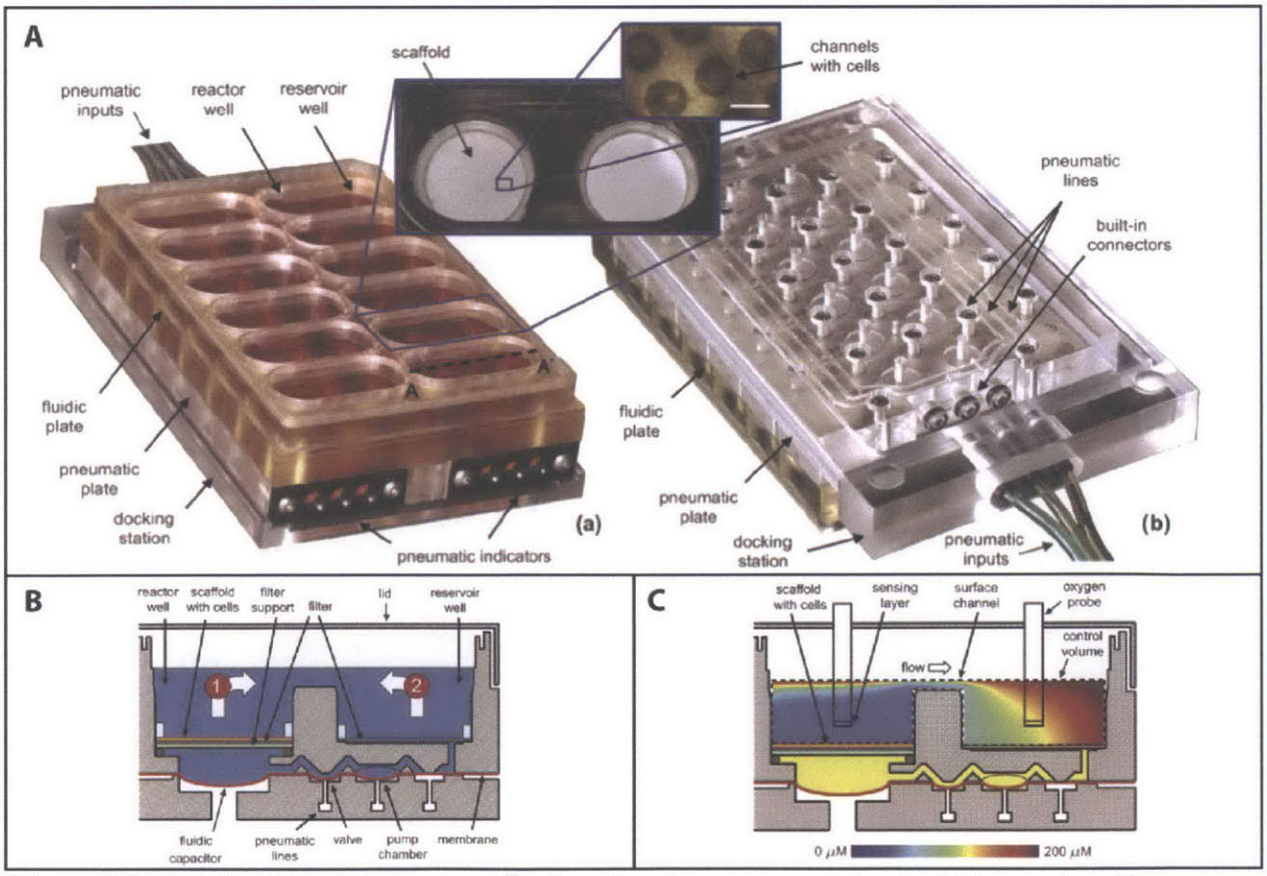

Figure i.1: Existing liver bioreactor. Twelve chambers are contained within a polysulfone platform, each of which has an isolated circulating media flow actuated by a lower pneumatic

platform (A). Flow can be made to flow in a clockwise (up through scaffold) or counter-clockwise (down through scaffold) direction (B), which can be used to culture and seed cells as desired. The chambers have been designed to provide high levels of oxygen delivery to the cells with relatively low flow rates, generating chemical and mechanical conditions similar to those found in vitro (C).

The main body of the device consists of a polysulfone micro-machined structure that contains 12 wells, each of which can accommodate a single tissue scaffold. These scaffolds are perfused via independent circulatory loops powered by miniature pneumatic pumps in the lower portion of the platform (acrylic, on right in Fig. i.1a) controlled via programmable external air pressure lines. The lower portion of the image shows modeling of media dissolved oxygen in the fluidic circuit (culture flow is clockwise in this image). The scaffolds in the original published work consisted of silicon or polystyrene wafers, 250um thick, with 300um diameter holes drilled into them, placed on top of a filter with 1-5um pores. Cells are suctioned down into the drilled microwells via downward flow, and once they have coalesced against the filter and anchored themselves, the flow is reversed. Over time, the cells align themselves to allow unimpeded media flow through the microwells. Figure i.2 shows the constructs at this point in a silicon scaffold (A) and in a hydrogel scaffold (B).

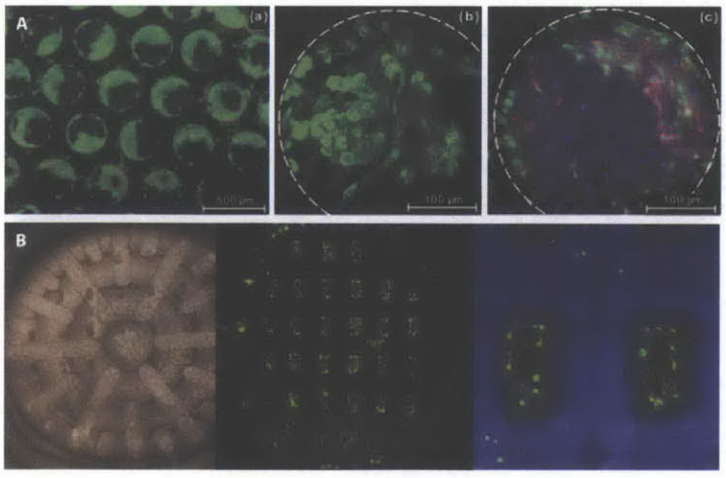

Figure i.2: Existing microwell scaffolds with seeded cells. (A) Early scaffolds consisted of silicon wafers with drilled arrays of holes 250um in diameter; scaffold is black in image, cells

are green. Bioreactor driven flow causes the cells to self-organize to allow flow through central channels. Similar scaffolds have recently been made from hydrogel materials, which present a better mechanical environment for the cells (B).

Continuous media perfusion is necessary to ensure adequate mass transport and nutrient delivery, as liver cells are highly metabolically active. In the body, however, hepatocytes experience little to no fluidic shear stress, and excessive perfusion can cause a loss of cell morphology and function. It is therefore important for any liver bioreactor to appropriately balance these competing demands and devise ways to uncouple these two parameters.[9-14]

i.3 Native liver tissue

Native liver is very dense, regularly organized, and thoroughly vascularized. Figure i.3a shows histology of the functional unit of the liver. Each functional unit (liver lobule) is roughly 600-800um across. Hepatocytes are large cuboidal cells, on the order of 20-50um in diameter. i.3b shows a three-dimensional schematic of a lobule. The hexagonal shape in the schematic is not a simplification – lobules in native tissue are arranged in a startlingly hexagonal fashion, with the corners of most hexagonal units containing a portal triad of an incoming portal vein (blood from the gut), incoming hepatic artery (oxygenated blood from the systemic circulation) and draining bile duct (leading to the intestine). The two incoming blood flows blend together in the microvasculature of the liver, called the liver sinusoids, which collectively drain into the large hepatic vein in the center of the functional unit.

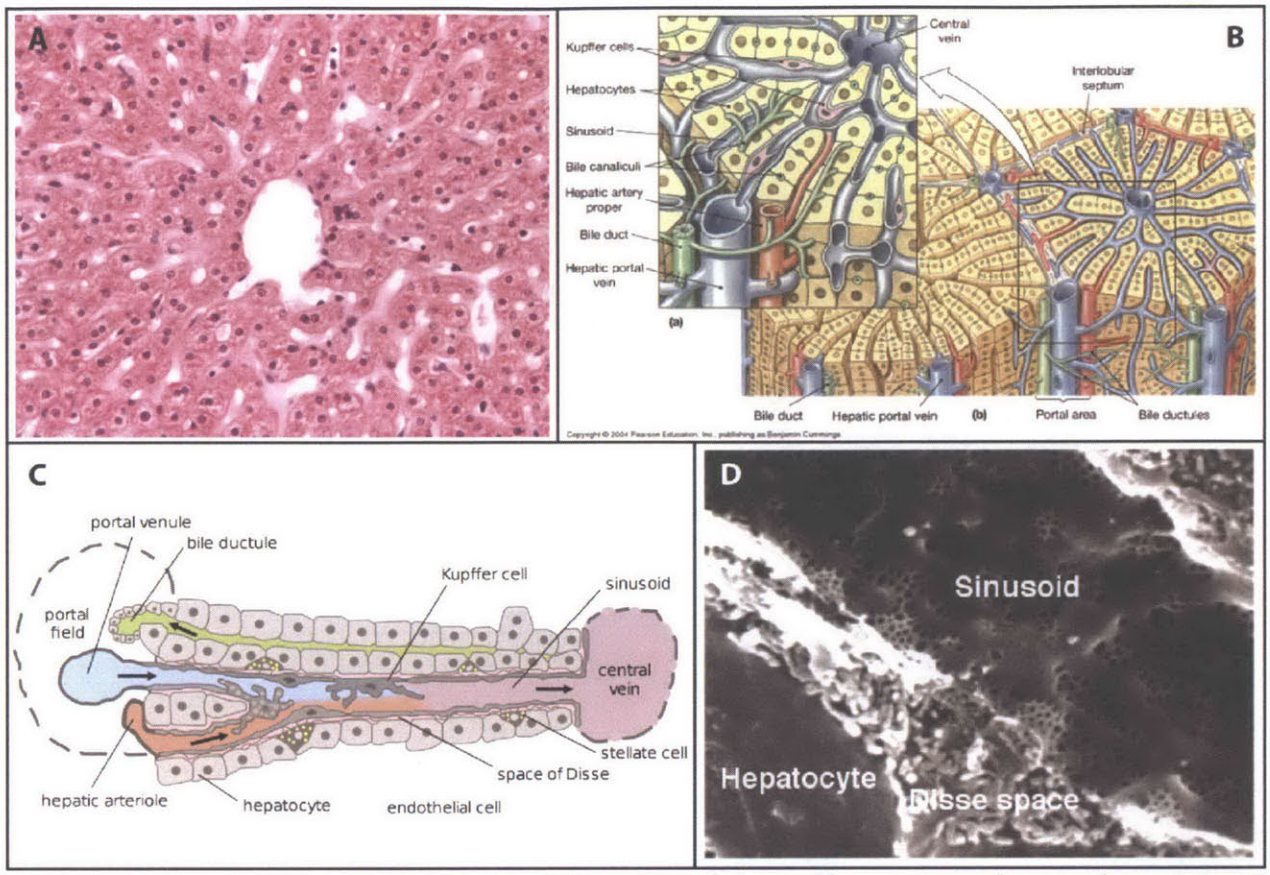

Figure i.3: Histology of the liver. (A) An H&E stained slice of liver tissue, showing hepatocytes, endothelium, sinusoids (white pathways) and central draining vein. (B) A schematic detailing the complex vascular architecture of liver tissue lobules. (C) A zoomed-in schematic showing the cellular and matrix organization of a single sinusoid. Note the space of Disse drawn in pink, which is filled with extracellular matrix that separates the vascular and parenchymal compartments. (D) An SEM micrograph of freeze-fractured liver tissue showing the nano-porous matrix in the space of Disse and the highly fenestrated endothelial cell layer.

The blue cells in i.3b represent hepatic endothelium, which line the entirety of the vascular system in the liver, including the sinusoids, and are fenestrated, as can be seen in i.3d. The fenestrations in the endothelial layer allow fluid flow out of the capillaries and into the interstitial space around the hepatocytes. This bathing of the hepatocytes is essential to liver function, as it allows the liver cells to modulate blood content, absorbing, metabolizing, and secreting various molecules as necessary. Any vascularized liver scaffold needs to take this into account.

Figure i.3c shows a detail of a single sinusoid. Of particular note is the space of disse drawn in light pink. The space of disse is a partial basement membrane of extracellular matrix that separates the vascular and interstitial spaces in the liver. A close-up view of the matrix in this region can be seen in the SEM micrograph (i.3d). The matrix in this space defines the overarching architecture of liver tissue, and creates a functional barrier separating the vascular and epithelial regions in the organ, effectively dividing the tissue up into two cellular compartments that are in constant communication due to the porosity of the extracellular matrix. This ECM structure is the component of the tissue that this thesis has most directly sought to synthetically replicate. If a structure could be built that replicated this three-dimensional architecture, allowed spatially-segregated cell seeding, and allowed appropriate fluidic communication between the interior and exterior of the small vessels, we would have the tools in hand to create working tissues with histologic structure in the laboratory.

i.4 Initial tissue designs

Figure i.4 shows proposed CAD designs for a micro-fabricated scaffold that mimics native liver architecture. Fig. i.4a-b shows a profile and 3D rendering of the vascular basement membranes in a single liver sinusoid. Particular care was taken to attempt to replicate the scale of the tissue. Sinusoids were drawn as 10um diameter conduits, with the diameters of larger vessels calculated to accommodate the volume of all incoming vessels. The 3D rendering Fig. i.4b was drawn with 1um walls, 40um corner arteries, and a 100um diameter center vein. Hepatocytes would be seeded into the open spaces between tubes, and, if desired, endothelial cells could be selectively seeded into the luminal spaces, provided that a patent cell delivery path was available. By selectively capping the ends of various tubes, flow could be forced into the corner vessels, through the capillary networks, and out the center vein. Although modifications would have to

be made to actuate this flow pattern (e.g., pressure-maintenance tapering), this model acted as a first-principle concept design.

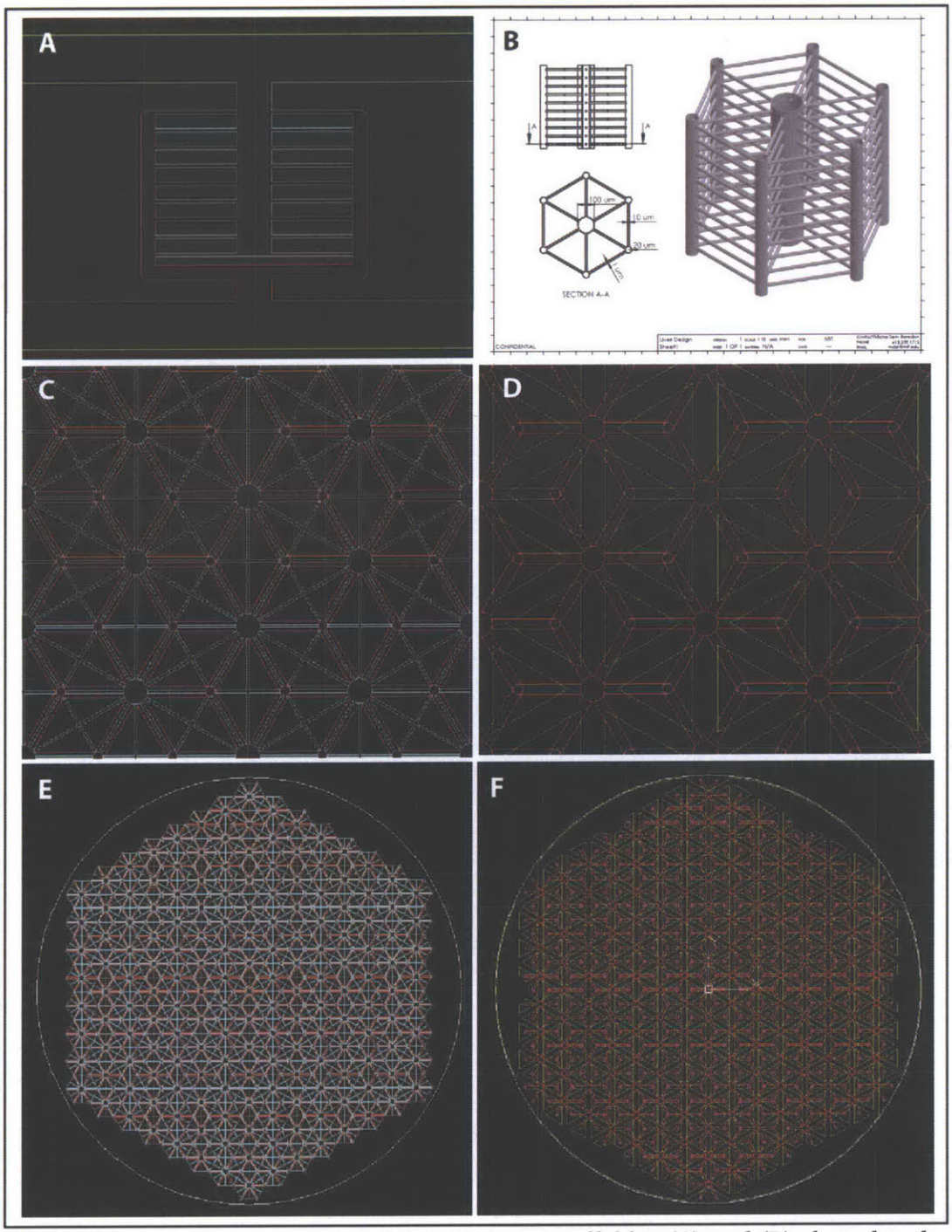

Figure 1.4: Proposed designs for microfabricated liver scaffolds. (A) and (B) show details of a single lobule model, scaled to be physiologic with 10um capillary diameters and 1um basement membrane walls. (C) and (D) show top-down views of a space-filling array of these lobules, showing the capillary-level fluidic network in blue (C) and larger media delivery networks in

green and red (D). (E) and (F) show large arrays of these units within an 8mm diameter circle – a scaffold of this size would be ideal for culture in the existing bioreactors.

The colors correlate between the 2D CAD images. Fig. i.4c-d show plan-view details of the designs, and Fig. i.4e-f show space-filling models covering an 8mm diameter space, which would fill a single bioreactor well. Flow was intended to travel from the lower green network, into the smaller diameter red network, travel up the purple arterioles, and branch into and through the blue capillaries, before draining into the larger green network. These constructs were designed to be seeded top-down, as with the existing scaffolds. The thin isosceles black triangles in i.4c-d represent open space through the network of large green tubes; hepatocytes would filter through and fill the space between the blue capillaries.

i.5 Projection-micro-stereolithography

Structures like these have not been fabricated before. Many etching and casting based micro-fabrication techniques have been adopted by biological engineers from the electronics industry, in particular silicone/silicon casting; however these techniques are inherently two-dimensional in nature, as they require some form of templating and demolding. The construction of structures such as those shown above, with overhanging features in all three dimensions, explicitly requires a free-form fabrication technique. Material deposition 3D printing techniques tend to have a minimum feature size of 50-300um. To fabricate these structures, it would be necessary to perform localized 3D patterning of material in 1-5um^3 increments.

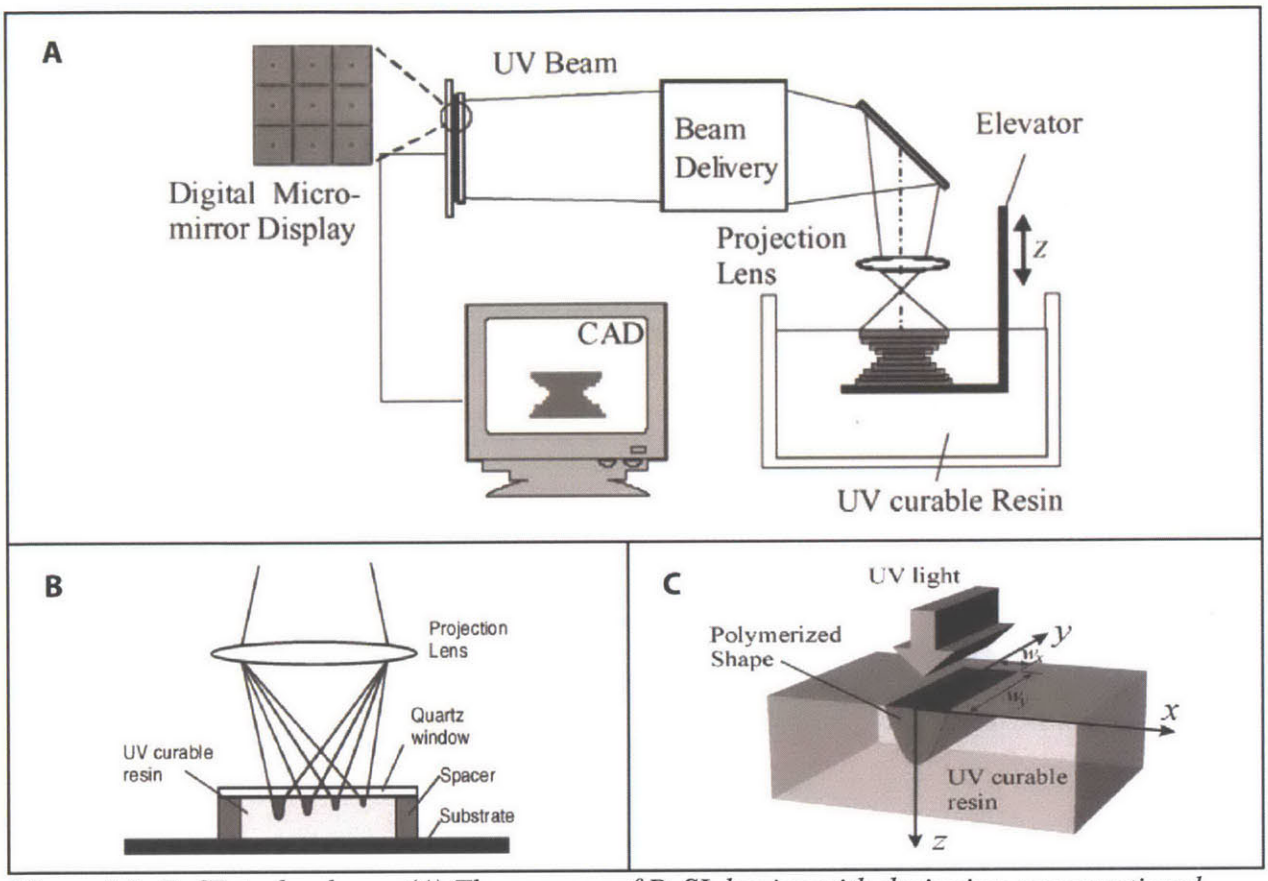

Figure i.5: PuSL technology. (A) The process of PuSL begins with designing a proportional CAD model, digitally slicing and scaling that model. These slices are then sent one at a time to a dynamic mask (DMD chip). A series of optics shines UV light onto the dynamic mask, and a lens picks up the image in UV light and projects it onto the surface to be cured. If the curing surface it the upper level of a resin bath, the cured layer can be lowered, and an additional layer printed on top. This process is repeated until the entire original CAD model has been fabricated layer-by-layer. (B) A side view of cured features from a single exposure beneath a fixed print plane. If the print plane is made from an oxygen absorbing material, the cured features will not anchor to the upper print-plane and the part can be lowered. (C) A schematic showing the approximate shape of cured material from the exposure of a single pixel line. The resulting features shows a Z-X plane Gaussian form.

Very recent advances in materials processing allow this resolution to be achieved. The laboratory of Dr. Nicholas Fang, in the Laboratory for Manufacturing and Productivity at MIT, has rigorously developed techniques associated with a form of fabrication dubbed projection-micro-stereolithography (PuSL). Figure i.5 shows a schematic of the process (images courtesy of the Fang group). PuSL uses patterned light to cure UV-reactive polymer resins in ascending layers and build up a three-dimensional part. First, a 3D CAD file of the part is generated and

sliced into layers. Each layer takes the form of a bitmap image that is relayed to a dynamic mask, either a Digital Micromirror Display (DMD or DLP) or Liquid Crystal on Silicon (LCoS) chipset. A UV light is shined onto this chipset, which contains a then reflective pattern, and the resulting image is projected onto the surface to be cured by a projection lens. High-aspect ratio vertical dimensions are achieved by curing the top layer of a resin bath against a submerged substrate that can be progressively lowered after each layer is exposed/cured. If a reducing lens is used, a bitmap image that would fill a 1920x1080 resolution computer screen can be shrunk down to ~2x1mm, leading each pixel of the sliced image to correlate to a point of light less than one micron across. With the right choice of equipment, experimental parameters, and polymer resins, extremely small feature resolutions can be achieved.[15-23] An excellent paper on this topic was published in 2005 by Sun et al., and is a superb reference for readers interested in learning more about the mechanics and subtleties of the PuSL fabrication technique; many of the images discussed in this section were originally published in this manuscript.[24]

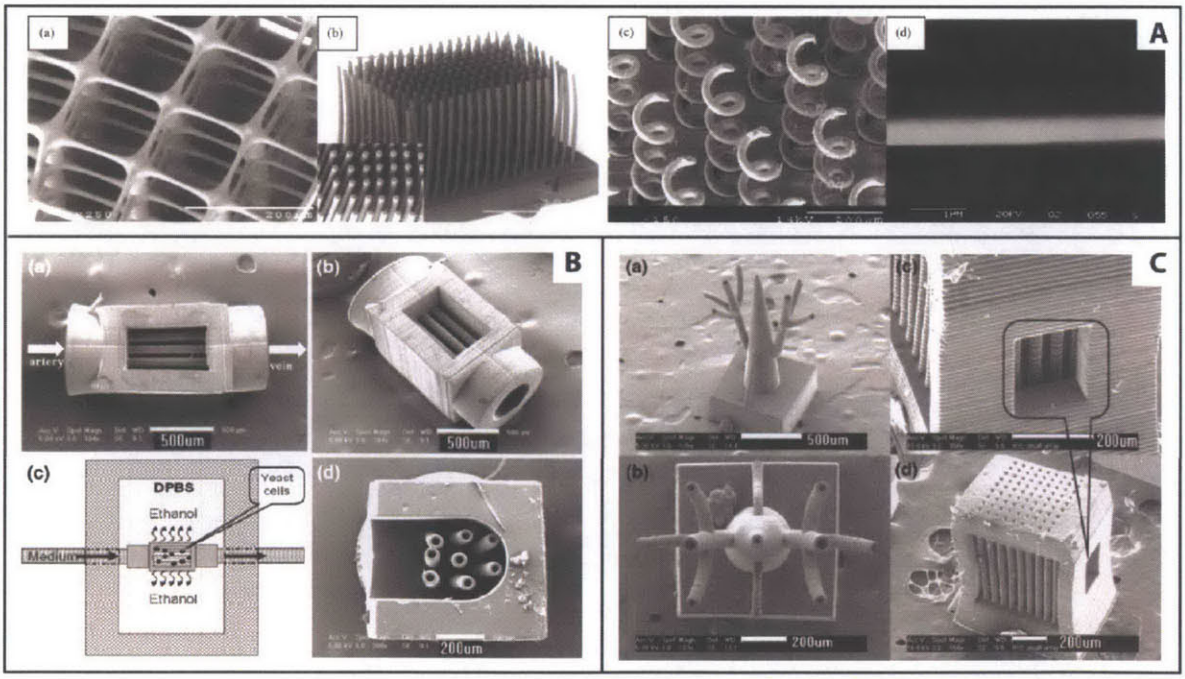

Figure i.6: Parts previously fabricated with PuSL. (A) shows feature resolution demonstrations. Particular note should be taken from the right-most image; this is a 0.6 micron diameter wire

made from a single exposure against a glass slide. (B) and (C) show attempts at making biologically-relevant strucutres. (B) shows a needle-cannulatable microscaffold designed to culture yeast cells. (C) shows hollow, branching fluidic architecture, along with an additional attempt to make linear capillary-like strucutres. Images taken from Sun et al. and Xia et al.[24,25]

Figure i.6 shows a collection of fabricated parts that have been previously published by the Fang group. The first row shows a collection of structures that demonstrate the high-resolution capabilities of PuSL, including complex overhanging structures, high vertical fabrication aspect ratios, and in Fig. i.6a, the ability to make sub-micron positive features (shown on far right is a suspended cable about 600nm in diameter). Figures i.6b-c show previously built structures hinting at the impact this technique could have on tissue engineering. Fig. i.6b shows a miniature bioreactor, published in 2009, used to culture yeast cells, with two ports for injection needle cannulated flow, a series of 40um diameter "capillaries," and an open wall to allow cell seeding. Shown in Fig. i.6c is a demonstration of PuSL-fabricated three-dimensional branching fluidic architecture, and a slightly larger version of the first miniature bioreactor, built without flow cannulation points.[25] From these images and publications, and after discussion with Professor Fang, it was concluded that it was theoretically possible to build structures similar to that shown in Figure i.5 using PuSL.

i.6 Polymer resin demands

The material constraints and demands for this system were known in advance to be fairly specific. To work with the PuSL technique, the material, or mixture of materials, had to be fluid and relatively non-viscous at room temperature. It also needed to cure locally and quickly, to allow small feature sizes and acceptable build times, and it needed to be non-toxic both before and after curing. Predominantly, it had to freely allow the diffusion of oxygen, glucose, cytokines, and large molecules such as serum albumin (~100nm diameter). Finally, the material should also be hydrolytically degradable over weeks to months, which would allow seeding of

cells and then gradual replacement of the synthetic matrix with natural cell-produced ECM. Originally, the concept was to use poly-lactic-co-glycolic acid (PLGA) to fabricate these scaffolds. However, as will be discussed further in Chapter 2, other materials have also proved promising and easy to work with, and have been investigated in parallel.

i.7 Thesis organization

This project had multiple components and therefore demanded simultaneous avenues of investigation. The first chapter of this thesis details the design-build process undertaken to construct a programmable projection-stereolithography apparatus designed specifically for tissue engineering. The second chapter discusses development and optimization of a set of resin mixtures that can be used with the machine to create viable scaffolds. The third chapter reviews designs and fabrication techniques for different types of scaffolds that have been pursued during the past months, following completion of the machine. There is significant chronological overlap among the three chapters, as work was done for each of these lines of investigation throughout the past two years, and findings from each line of inquiry affected the others.

Chapter 1: Design and fabrication of a PSLA apparatus tailored for in vitro tissue engineering

Introduction

It is a powerful tool for biological engineers to design and fabricate their own equipment for a specific aim. At the commencement of this project, we had the opportunity to design a PuSL apparatus explicitly for tissue engineering applications. This meant choosing specifications that would allow the proper resolution for our intended designs, and the proper build area/volumes for the construction of macroscopic structures that could be seeded with cells and integrated into the existing bioreactor platform. It also meant building long-term flexibility into the design, laying out a foundational architecture that could be modified over years of work to suit changing research needs.

Although the process in this chapter will be presented as a linear progression, in reality the design of the machine affected component choice and vice-versa. The development of task-specific equipment is a complex process that necessitates long-term vision and recognizing that physical design choices have the potential to negatively (or positively) affect experimental ability. Particular attention was paid to making sure that the machine was capable of fabricating parts larger than those previously made for the liver bioreactors, as the appropriate scale for different tissues within the BIO-MIMETICS project was not yet known.

1.1 Design considerations

It was important that prior to sourcing components for the SLA machine, conceptual designs existed for each of the potential scaffolds that the lab might want to make, as the specifications and spatial arrangement of each active component within the apparatus (stages, light source, chipset, optics, etc.) would effect the resolution, speed, and scale of fabrication. As

discussed in Section i.4, initial scaffold proposals had been drafted. Therefore the foremost step was assembling a machine that would be capable of building similar structures while being flexible enough to satisfy changing demands during coming years of research. Key functional parameters have been laid out in Table 1.1.

Table 1.1: Functional parameters of PuSLA for tissue scaffold construction	
Resolution (XY)	< 2 microns
Resolution (Z)	< 0.5 microns
Completed build size	8-60mm diameter, 1-20mm deep
Motion repeatability	< 0.250 microns
Speed of fabrication	< 1 exposure cycle per second
UV Light	365nm, high intensity
Material handling	Minimal fluid volume for application Compatible with PEG, PLGA, PCL, PLA, EG, initiators, acrylates and methacrylates, common solvents

In addition to satisfying demands for resolution, stage repeatability, UV intensity, scaffold build scale, and speed of fabrication, it also was deemed important to have two sets of optics that would allow fabrication on multiple length scales. Having one lens with a 1:1 projection ratio and one with a 10:1 reduction ratio would allow fabrication of scaffolds with positive XY features on a continuous range from 1um to 1cm. This would allow the PuSL to be useful for ongoing efforts in the BIO-MIMETICS project while maintaining the capability to generate experimental scaffolds with much smaller feature sizes and complex architecture.

Replication of the resolution previously achieved by the Fang group was of high importance, as an aim was to construct capillaries similar in size to those found in the body, which are approximately 10um in diameter with 0.5-1um thick walls. Although functional designs could likely be achieved with larger positive features, minimizing the feature resolution of this system was a priority. At the same time, it was essential that this device be capable of printing relatively large parts via a step-and-repeat process, as a scaffold made with a single Z-stack of exposures would be at best ~1mm to a side, and would consequently be impossible to

work with manually or incorporate into the existing bioreactor platform. Many design decisions were guided by the need to minimize resolution but simultaneously maximize potential build size.

1.2 Component selection

Optics: A light source was purchased from Hamamatsu with a peak output at 365nm (Figure 1.1a). An LED light source was preferable, as it minimizes heat and vibration generation and eliminates the need for a computer-controlled shutter; the selected light source was pre-collimated to 40mm. A 1920x1080 resolution, 5um pixel-size, TI manufactured DLP chip and motherboard were taken from a commercial projector (Acer H6500), and selected cables were extended to allow the projector body to continue running the chipset (Figure 1.1b). A 10:1 reducing projection lens designed for high-resolution UV light transmission (Zeiss) was obtained from the Fang lab (Fig. 1.1c). This lens has a fixed object-to-image distance of 602mm, which meant that the secondary lens needed to be able to replicate this image-to-object distance while producing a 1:1 projection ratio. A suitable (non-UV optimized) lens was purchased from Canon (Fig. 1.1d). Most additional optics were purchased from Thorlabs or Edmund Optics. These parts included a beam splitter, camera, beam expander and collimator, UV-coated mirror, and assorted optical positioning equipment.

Table, computer, stages: A vibration-damping and self-leveling 12" optical table was purchased from TMC. As the PuSL process would require the processing of complex three-dimensional CAD files and thousands of bitmap images, a dedicated computer was purchased from Dell with an emphasis on processing power, graphics performance, and storage capacity. Three linear encoder crossed-rolled bearing stages were selected from Aerotech to perform stitch-and-repeat builds. These stages would allow 50nm step sizes in all three directions and a repeatability (crucial for stitched parts) of approximately 250nm (Fig. 1.1e).

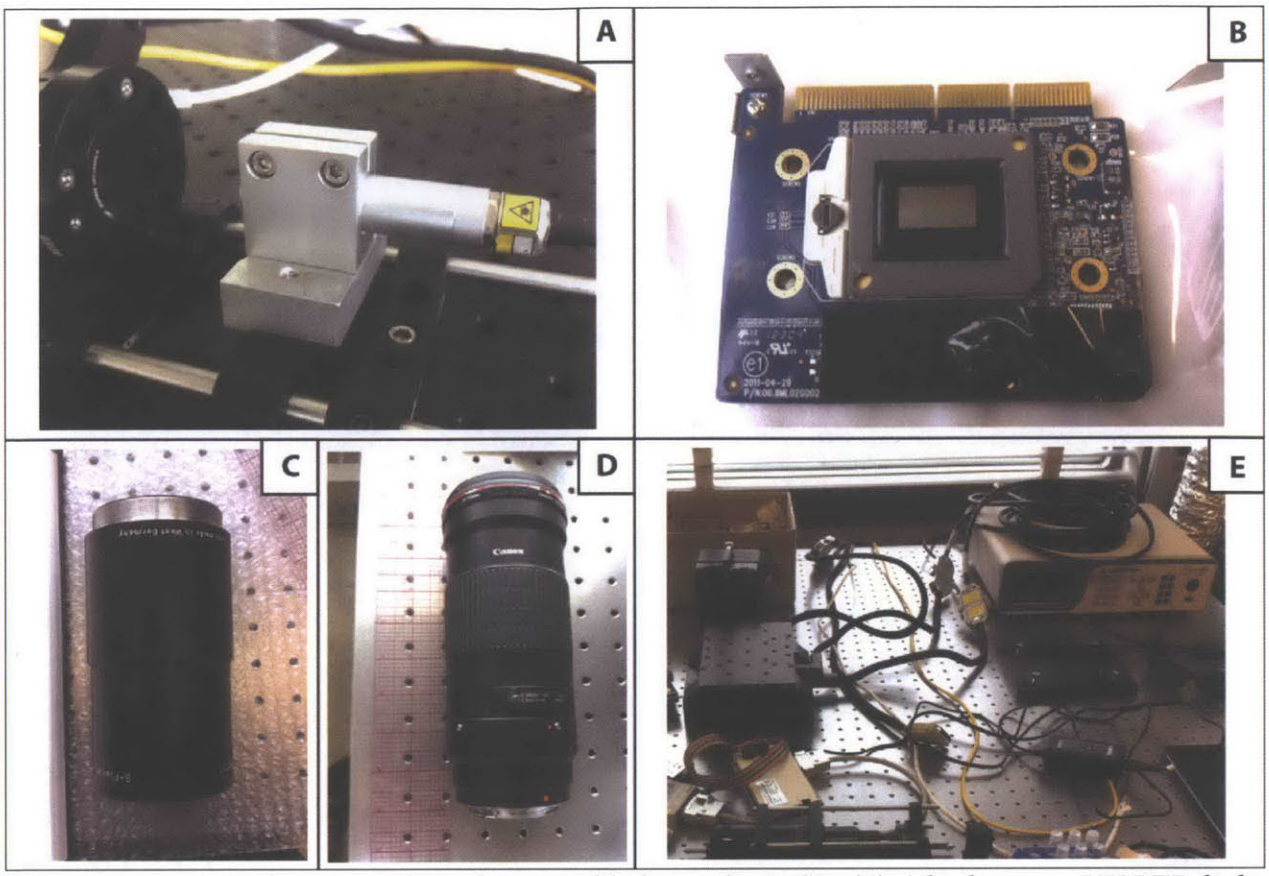

Figure 1.1: Selected components to be assembled into the PuSL. (A) A high-power UV LED light source with custom specifications. (B) The DMD chip to be used. The small reflective patch in the center has a 1920x1080 micromirror resolution – each mirror is 5um^2. (C) shows the hand-made Zeiss 10:1 reducing projection lens, specially coated for UV transmission. This lens has a fixed focal length and largely defined the spatial layout of the system. (D) shows a high performance lens purchased from Canon to provide 1:1 reduction ratio projection over the same distance. (E) shows the motion stages selected for this project, to provide both Z platform actuation and XY exposure stitiching. These stages are high performance linear motion stages, capable of 50 nanometer steps sizes over a distance of 30mm.

1.3 Technical drawings

Technical drawings were developed for the apparatus prior to fabrication and assembly, views of which can been seen in Fig. 1.2. The layout of the PSLA was built around the spatial demand that the DMD chip and print plane be 602mm apart and highly parallel, a constraint dictated by the Zeiss lens and lack of autofocus stage. A suspended upper table top was drawn to support the main optics at this elevation relative to the print plane, with an aperture cut to allow the intended light path. The optical alignment was dictated by the DMD chip, which was found

via laser-alignment testing to only direct light perpendicular to its face if the incident light is 24 degrees from normal and on a 45 degree plane relative to the chipset; this implies that an "on" micro-mirror tilts 12 degrees, and that the square mirrors flip diagonally. These and other design constraints are represented by construction lines in Fig. 1.2.

Figure 1.2 (on next page): Technical drawings of apparatus to be built. (A) shows a front elevation view with all components properly aligned. The print plane and DMD chip elevations were fixed in space; they are shown as horizontal construction lines. The light path is shown by the upper diagonal construction line and the broad cone connecting the DMD chip and lens. Swinging mechanisms were designed to allow repeatable manual positioning of two different lenses. (B) A side-elevation view. (C) A top-down planar view. Note the 45-degree oriented light path not well represented in the upper image.

A - Front elevation

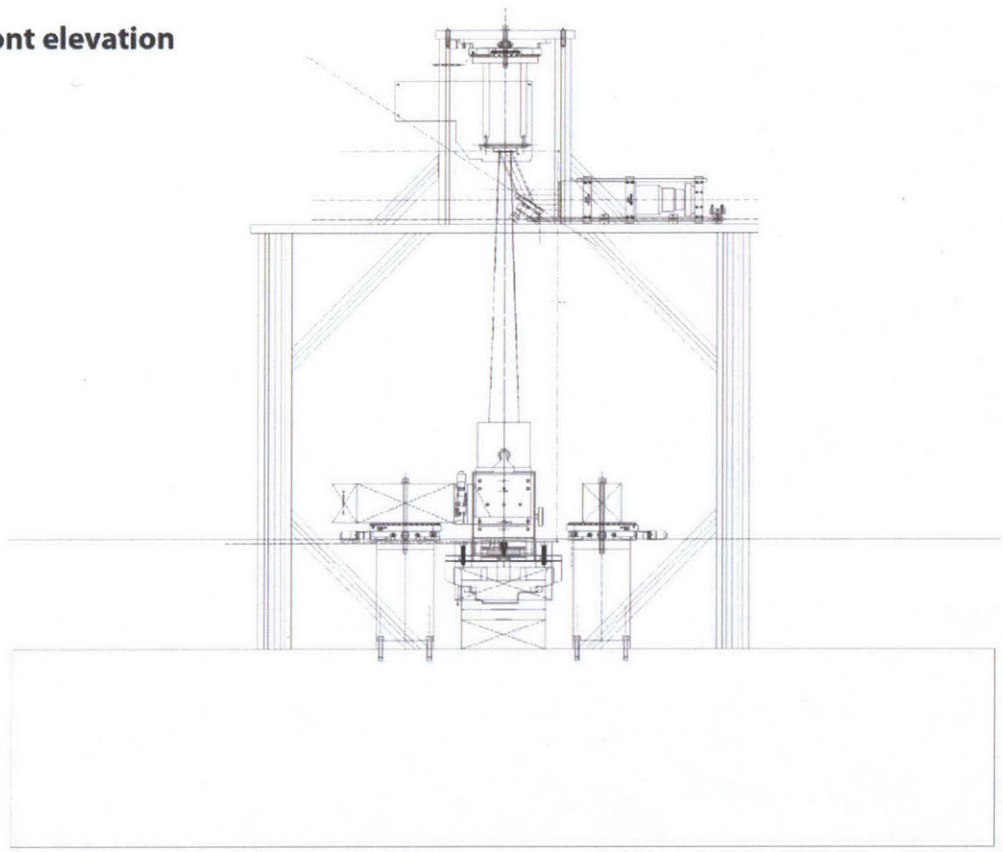

B - Side elevation

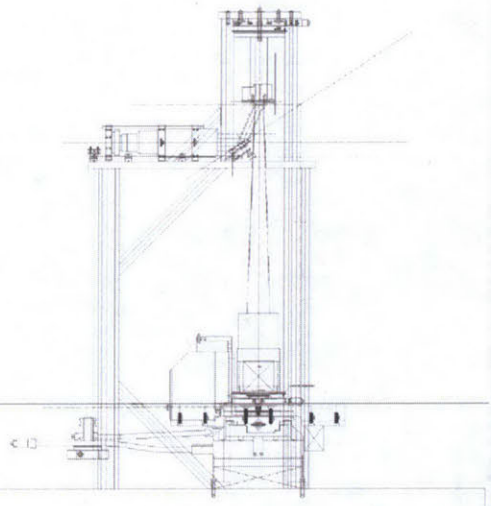

C - Plan view

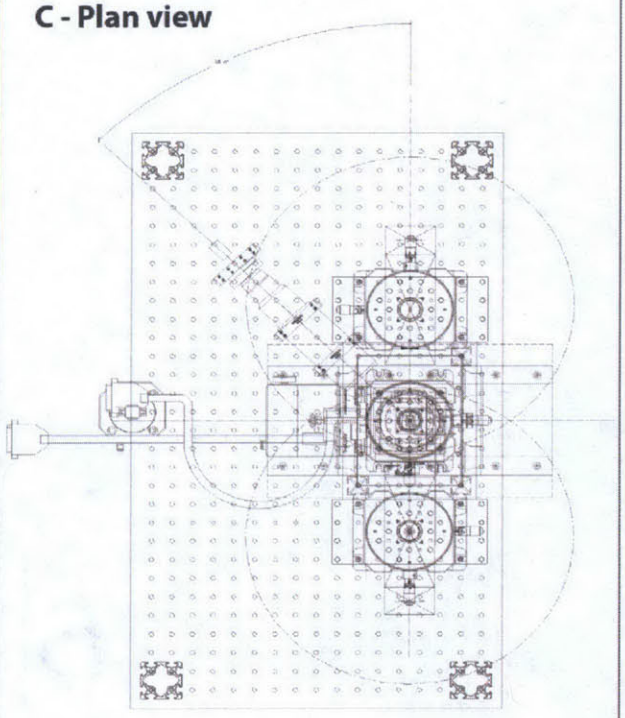

The closeness with which the stages were placed relative to one another would affect the accuracy of fabrication, with closer stages producing more precise builds, due to the minimization of abbe, or sine, error, in which angular misalignments are amplified by long swing arms. To minimize potential resolution, but maximize potential build area, three separate stage-and-piston subdesigns were drawn, which can be seen in Fig. 1.3.

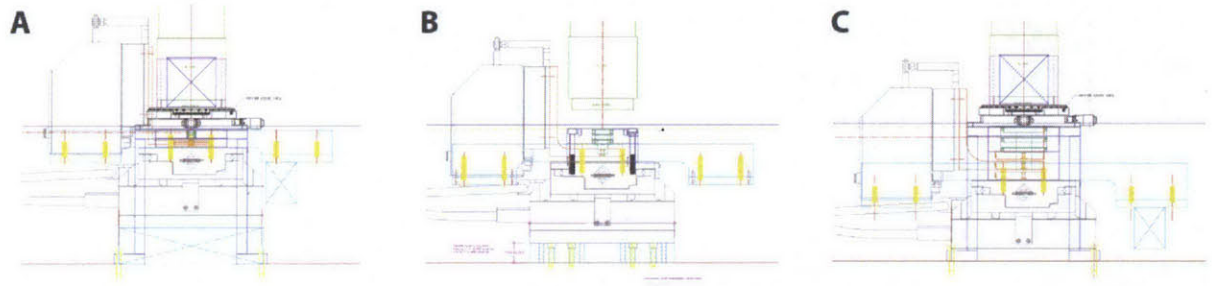

Figure 1.3: Three interchangeable piston sizes and assemblies. Note that the print plane (blue line) and table-top (red line) are always equidistant, allowing independent swap-out as necessary. The assembly shown in (B) was eventually chosen for fabrication; future research demands may necessitate the fabrication of the larger assembly shown in (C).

The small piston (Fig. 1.3a) allowed a build volume 5mm deep and 1cm in diameter, the middle piston (Fig. 1.3b) a build volume of 0.5" deep and 1" in diameter, and the large piston (Fig. 1.3c) a build volume of 2cm deep and 6cm in diameter. As can be seen by comparing these images, the print plane was elevated above the table sufficiently to be fixed relative to the table-top while allowing interchangeable pistons assemblies, as it was not known in advance which was likely to be the best option. Following technical layout, a three-dimensional drawing set of the apparatus was generated prior to fabrication. This can be seen in Figure 1.4.

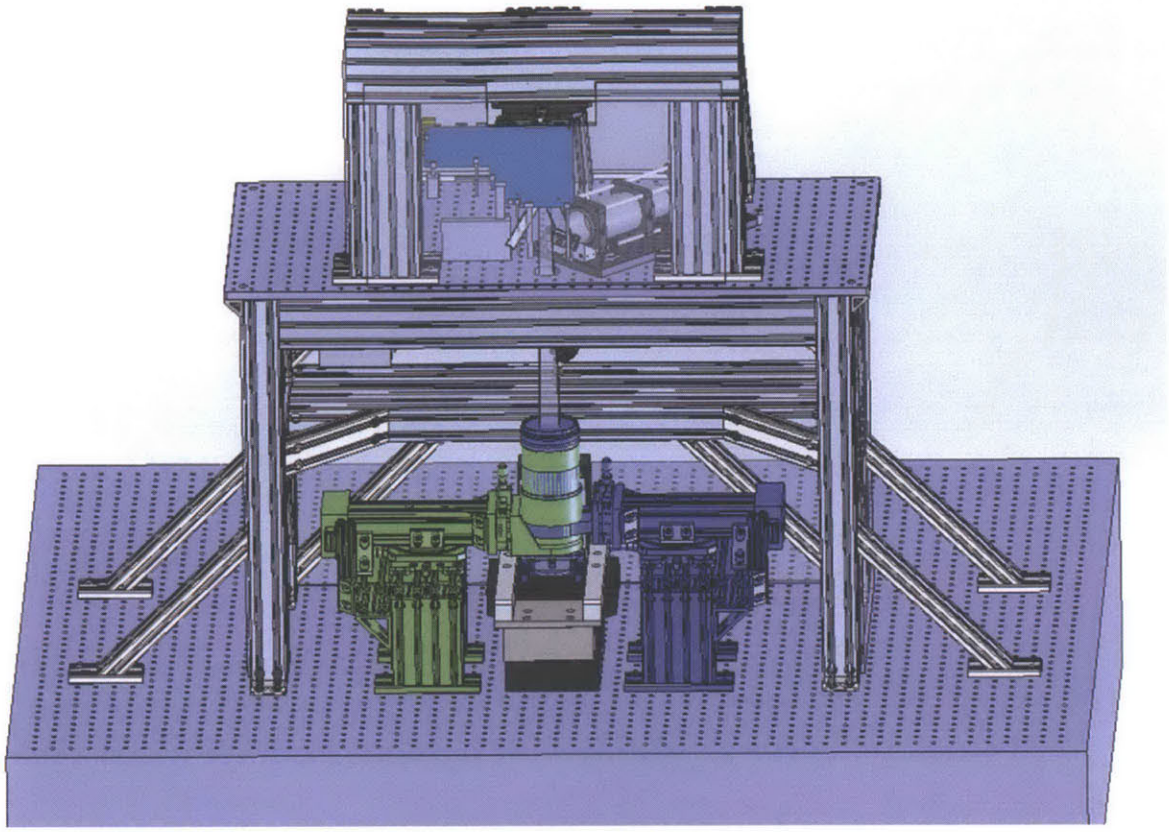

Figure 1.4: A Solidworks rendering of the PuSL to be built. Additional structural bracing was added by a consulting engineer to help eliminate vibration effects. Drawing shows the two lenses superimposed on each other. The lens-rotation features shown here were redesigned to allow ease of operation.

1.4 Fabrication, assembly, and optical alignment

All custom components were fabricated by either the MIT central machine shop or the researcher himself. Stages of assembly can be seen in Fig. 1.5. The drop bars were mounted first to the surface of the optical table. The upper table-top was then mounted, and adjusted to match the level of the lower table surface. Once the upper table was in place, the DMD chip assembly, LED, and assorted optics could be fixed and appropriately adjusted. The stages were then mounted below, along with the 1" diameter piston assembly that was chosen for fabrication.

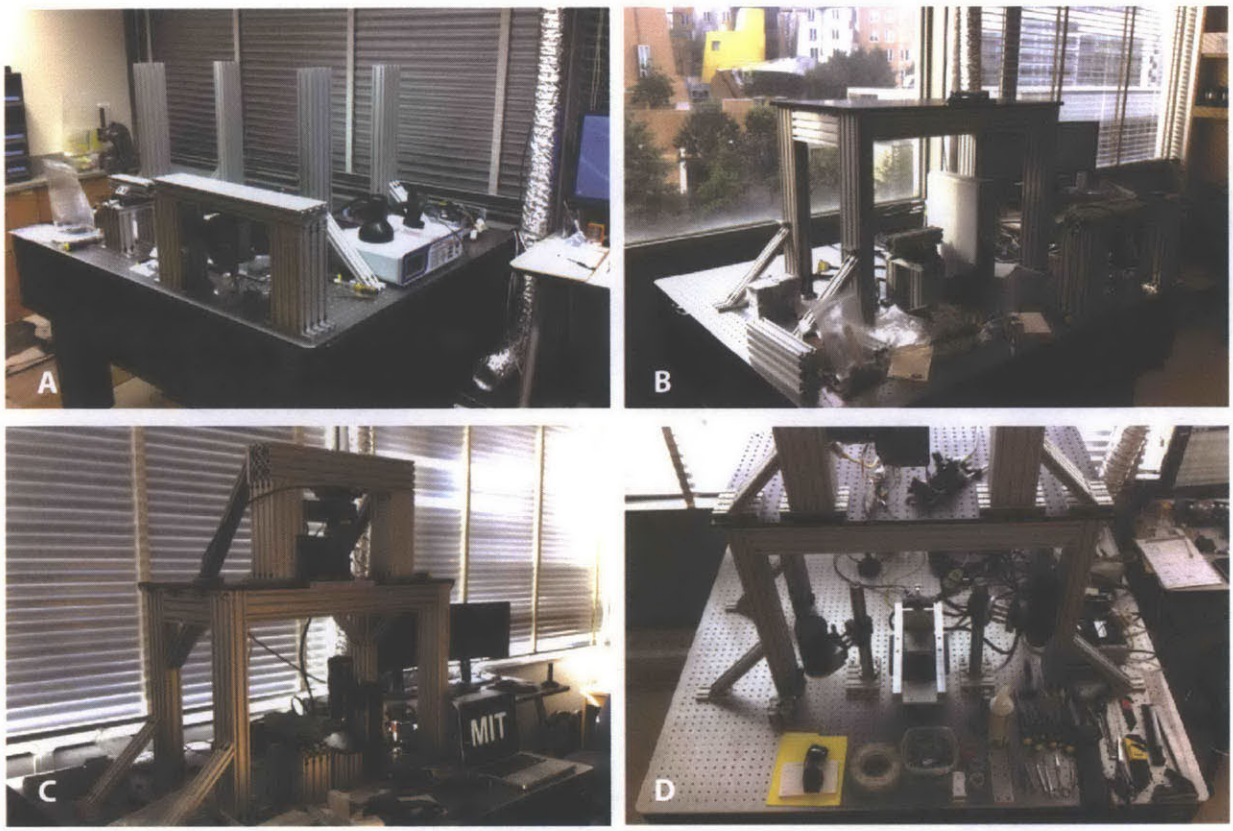

Figure 1.5: Assembly following parts fabrication. (A) The drop-bars were installed first; these were machined to a height within 0.0001". (B) Mounting of the upper table top; care was taken to level this with respect to the lower table-top. (C) Initial optical mounting and calibration. (D) The final system assembled. Note the central stages, dual swinging lenses, upper calibrated optical assembly, and computer on the far right which controls all non-manual components.

Proper optical alignment was critical for smooth operation. In many optical systems, a stationary water surface is used as a reference to align a vertical laser. In our system, however, the print plane would be dependent not on gravitational level, but rather the slope of the stages themselves, however slight. The optics therefore needed to be aligned with a laser projecting upward normal from the mounted stages. To achieve this, a three-axis laser level was mounted to the print plane, projecting a vertical beam aligned with the center of the XY motion travel range. With the DMD chip off, this beam was used to adjust the chipset until normal to the print plane, and then with the DMD chip on, was used to align the full set of optics, including the UV mirror, beam collimator, and UV LED.

1.5 Material delivery mechanism

Following assembly, it was determined that the original material delivery system would prove impossible to work with. Originally, material was meant to flow in through the stainless steel print-plane structure and travel through grooves in the surface, sealed by the PDMS/quartz glass print-window. Although this worked in principle, it was unacceptably messy, as uncured resin would escape from the channels following removal of the window. Accordingly, the PDMS print-window was modified to allow a through flow channel directly through the silicone, cannulated with 0.006" ID 316 stainless steel needle tubing. Fig. 1.6 shows images pertaining to this post-fabrication modification, including the portion of the machine in question and the casting process used to generate the material delivery channel in the PDMS print-window.

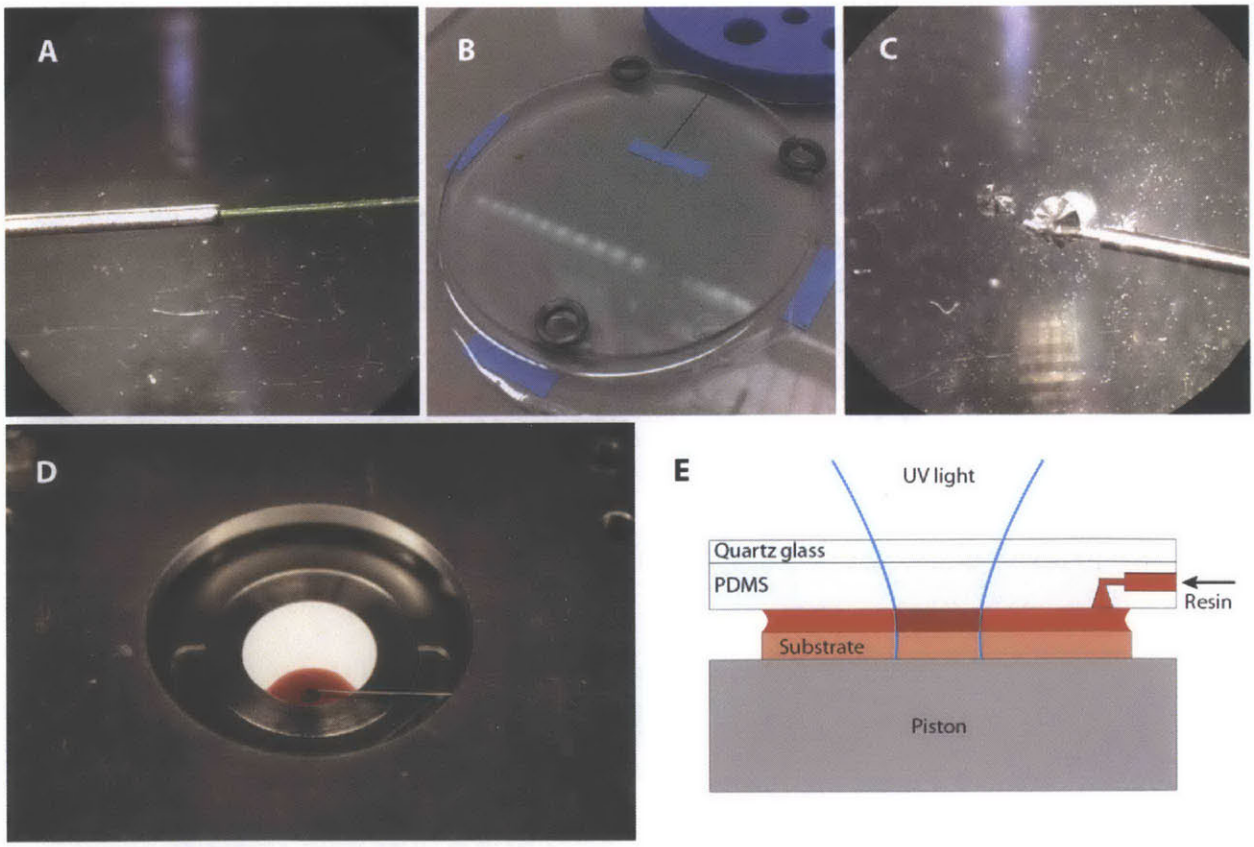

Figure 1.6: Print-plane development. The top-window needed both to act as a fixed, cure-inhibiting surface and to allow material delivery. To achieve this, 0.006" ID stainless-steel needle tubing was threaded with Teflon-coated wire, shown in (A) under a microscope. This

assembly was then cast in PDMS underneath a quartz glass plate. The needle and wire were then extracted, leaving a very small fluidic channel (C). For fabrication, the needle is reinserted without the inner wire, allowing cannulation and material flow onto the substrate without affecting the flatness of the curing surface. (E) is a side-view schematic of (D), showing resin in red and the substrate in pink. Substrates can be filters or glass slides with double-stick tape.

1.6 Programming, first operation, and assessment

The software to control the PuSL apparatus was developed using LabView. This software had to be able to send bitmap images to the DMD chip, control the LED light source, control the stages, and control the injection pump. The code to interface with the stages came with the Aerotech control module; the rest of the code had to be developed in-house. State-machine architectures proved particularly useful for this type of apparatus-control work; they consist of a case structure nested within an infinite WHILE loop, and they run continuously in the background until asked to carry out an action. This allows various buttons to be put in place on the front panel, each of which carries out a dedicated command and can be asked to pull from a set on input fields. State machines were developed to control image projection, LED exposure, stage movement, and material injection. A firstdraft of many iterations, these pieces of software allowed the basic testing of the machine. Further functionality was added to the code as needed on an experiment-by-experiment basis.

Initial experiments were carried out to validate the function of the UV-LED, optical alignment, operation of DMD chip, lens placement/alignment, XY stage function, injection pump response, piston alignment and operation, beam splitter alignment, camera focus, and timing of the LabView code. The first print made with the machine can be seen in Fig. 1.7.

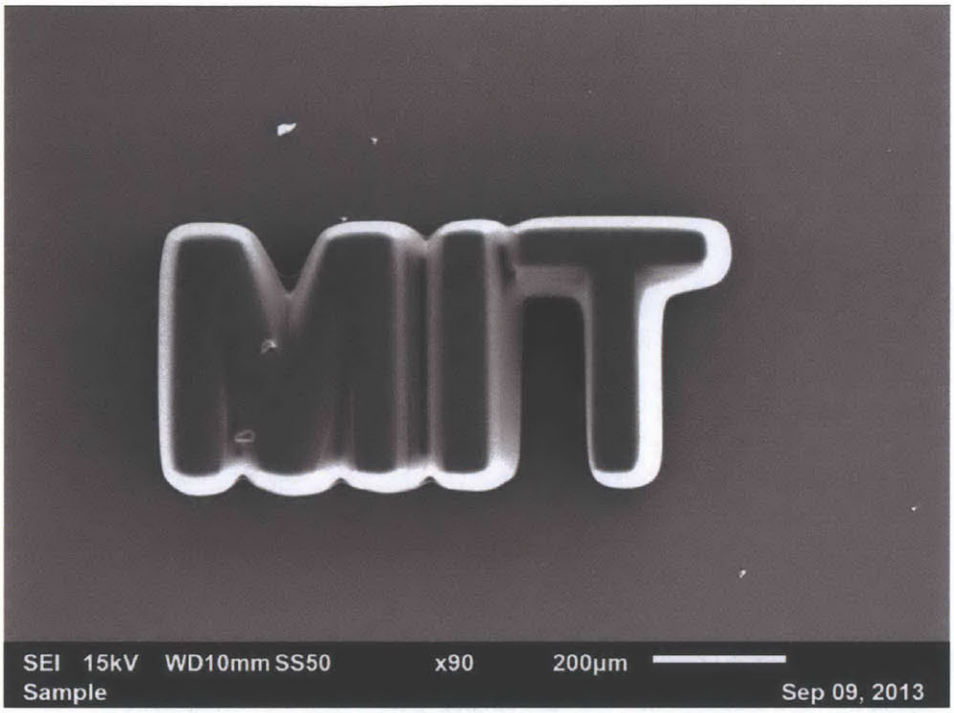

Figure 1.7: The first fabricated part made with the PuSL. Single exposure, PEGdma Mw 575 w/ 0.05% Sudan I, on glass coverslip.

Following completion of the machine it was necessary to assess some resin-independent parameters. The stages were tested by projecting repeating patterns of calibration grids at set spacings; the error in X,Y and Z positioning was so negligible that it was not measurable, even under SEM. The width of a single DMD pixel was found to correspond to a length of approximately 685nm using the 10:1 lens. The 1:1 lens contains a zoom that allows a range of magnification, but was generally set up to have a single pixel correspond to a length of approximately 9.0 microns, so that a single image would expose a 9.75mm wide area. It should be noted that the functional resolution of the system is dependent on the chosen resin and experimental parameters; as of the writing of this document, the minimum functional resolution of the system has not clearly been quantified, but it can be estimated at approximately 1-2 microns.

Conclusion

The final constructed apparatus has proven reliable over long time spans, and with proper coding can perform automated builds lasting many hours without researcher involvement. The resolution of the system is high, with single pixels theoretically able to generate sub-micron features. The motion stages appear to have been chosen well, and the UV LED light source is powerful, capable of curing small features in some resins in less than a second. A disadvantage of the chosen design is the reliance on PDMS as a building material – silicone is lipophilic and absorbs small molecules, which causes problems with a number of resin mixtures, as will be seen in the next section. Modifications to the design are ongoing, and the flexibility of the constructed system has been important to experimental success during this research.

Chapter 2: Development of resins for three-dimensional micro fabrication of tissue scaffolds

2.1 Introduction and Aims

The resins used in projection stereolithography have a strong impact on the properties of the fabricated structures. On a basic level, resin choice affects feature definition, cure and fabrication times, and cure depth. Each of these parameters, however, can be modulated by modifying experimental conditions such as exposure time, light intensity, etc. More importantly, the resin used affects the nanostructure of the fabricated parts.

The resins developed for this project had to satisfy three overarching criteria. First, they needed to work with the PuSL process, which meant being low viscosity and curing quickly and locally into a solid when exposed to UV. Second, as the intent was to create closed vascular networks in which the cells would be compartmentally separated from media flow, they needed to allow rapid diffusion of relatively large molecules, such as human albumin. These two criteria were absolutely essential to satisfy. Beyond these, it was also desirable to have hydrolytically degradable materials, which would dissolve over time during culture, allowing the cells to replace the lost polymer with biologically-made extracellular matrix. This meant that an ideal resin would be a fluid at room temperature, cure to form an open pore network with at least 100nm pore size, and if possible, degrade via hydrolysis.

2.2 Tools for assessment

As the majority of experimental work relied on knowing how various resin mixtures responded to different exposure times and light intensity levels, a LabView code was developed to allow rapid testing of these parameters, dubbed a "cure test." The algorithm prints an X by Y grid in the pattern of a typewriter, where the exposure time or exposure power is increased by a

set interval for each successive print; a 6x6 grid, for instance, could be used to test a range of exposure times from 0.1sec to 3.6sec in 0.1sec intervals.

This technique proved capable of revealing many pieces of information about a given material. In additional to establishing what exposure time was most appropriate to get robust features, simple grid patterns can give a sense of potential feature resolution. Materials with a high degree of reaction propagation show broadly spread, fuzzy features, in contrast to very thin gridlines made with higher-resolution materials. Since cure depth varies with exposure dosage, these cure tests can also be used to give an initial sense of cure depth for a material, assuming the substrate is reasonably level and the initial Z height is known. A standard cure test usually consisted of curing a 10pt line thickness 10x10 grid, 10um down from the print plane, in a 6x6 pattern with a cure time increment of 0.1seconds, larger if necessary. This procedure was used often and yielded many relevant data sets.

2.3 Mediating porosity

Natural extracellular matrix is nanoporous. It allows the transport of gases and small molecules such as glucose as well as larger proteins such as serum albumin. Visualizations of the extracellular matrix can be generated by stripping tissue of cellular material through detergent decellularization processes, dehydrating the remaining ECM in a fashion that preserves the micro- and nano- architectures, and then performing SEM or TEM. Figure 2.1 shows samples of lung tissue prepared and imaged in this fashion. The images shows that there is significant void space in the extracellular matrix, so that even while defining the organ architecturally and providing the majority of mechanical integrity, it acts as a minimal barrier to nutrient and chemical transport. It would be ideal to generate a resin that, when cured with UV light, generated a structure that had a similarly high degree of interconnected void space.

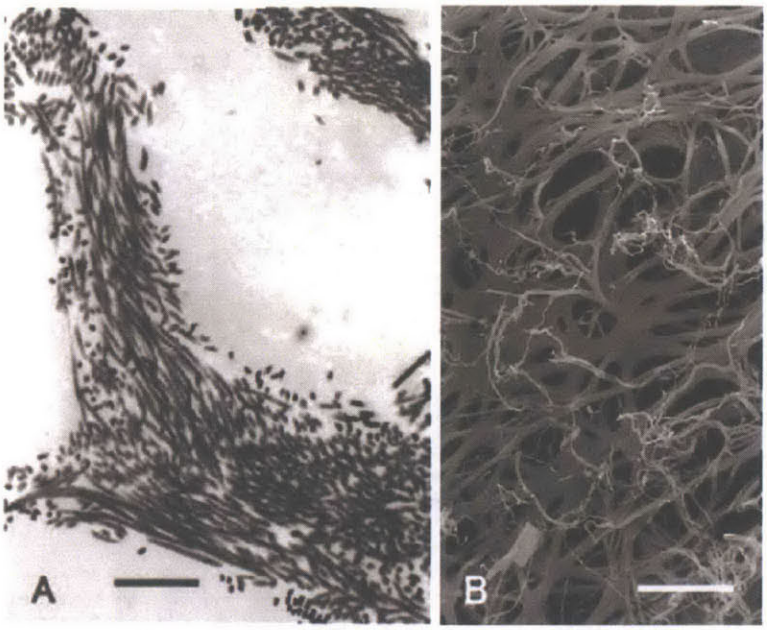

Figure 2.1: Nano-structure of native ECM. Scale bar in A=1um, in B=10um. (A) is a TEM of collagen in the vascular basement membrane of lung. (B) is a corresponding SEM of the elastin network. These two ECM proteins are fully intermeshed in this tissue, so the actual nano-porosity of the basement membrane is slightly less than seen in either image. The void-spaces in the collagen network define the pore size of the matrix in this tissue type. The large open areas in image (A) are the lumens of capillaries and alveoli; normally the walls of these lumens would be lined with cells. From Toshima et al.[26]

A promising tool already existed for this. Many two-part (or more) polymeric mixtures are known to undergo spinoidal decompostion under the right conditions, and the Fang group has previously harnessed this property to generate HDDA constructs with pores between 50-100nm. Figure 2.2 shows the principle behind this technique, and a sample of PuSL cured HDDA designed to emphasize this nanoarchitecture.

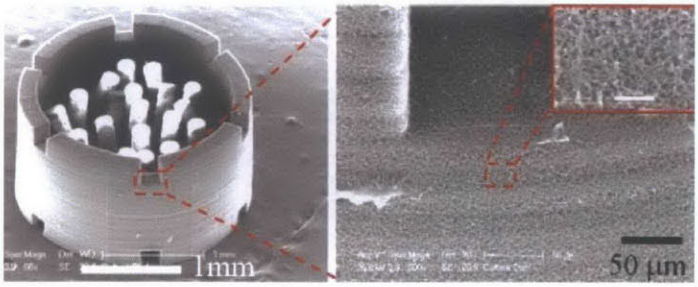

Figure 4.13 A micro structure fabricated in PµSL using a mixture of 50 wt% of HDDA and 50 wt% of PEG (MW250).

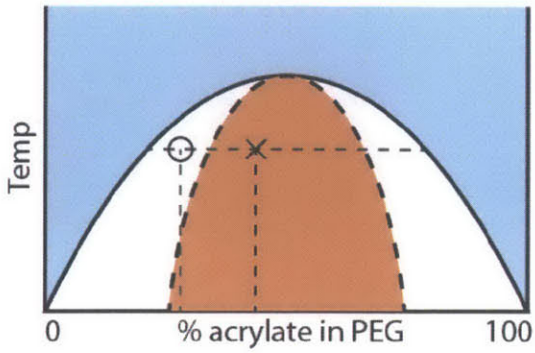

Figure 2.2: Nanoporosity with PuSL. The left image shows a structure fabricated by the Fang group demonstrating the ability of two-part resins to phase-separate into porous nanostructures upon curing. The theory behind this transition is diagramed at right. Shown in a temperature-composition phase diagram for a phase-separating binary system. UV exposure of an initally homogenous resin mixture rapidly increases the self-affinity of acrylate molecules, causing the mixture to phase separate in a ratio dependent on the resin composition and room temperature. If the composition is such that the sample falls within the spinoidal range (orange in image) it will undergo spinoidal decomposition, which displays an open-pore strucutre. The crosslinked acrylate becomes a solid, while the non-reactive PEG remains a liquid. Rinsing with water washes the PEG from the structure, leaving an open pore network.

Phase separation morphology was found to depend on the ratio of reactive to non-reactive material as expected. Fig. 2.3 shows bulk specimens of material with increasing PEG weight fractions; porous samples appear uniform opaque white due to light scattering. The surface and interior structure of similar samples can be seen under SEM in 2.3f-h. From these and other data it was determined that an ideal PEG weight fraction was likely ~50%, as these samples displayed mechanical integrity and interconnected pores on the order of 50-150nm.

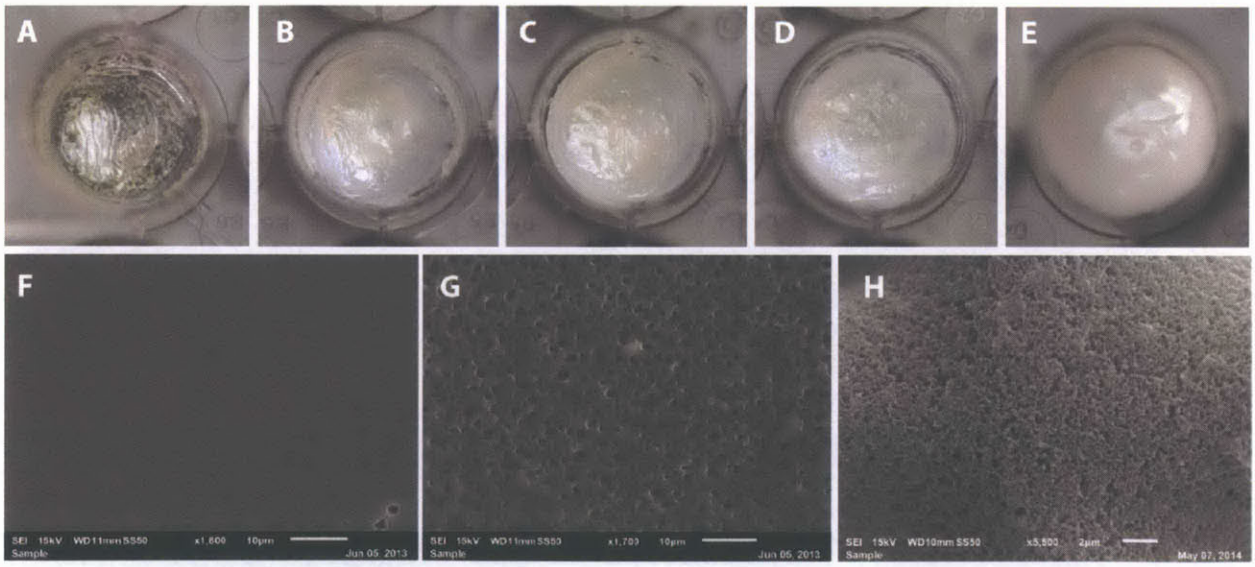

Figure 2.3: Composition dependence of porosity. (A-E) shows bulk samples of acrylate material (3-arm acrylate PEG, Mw ~428) with 0%, 20%, 30%, 40%, and 50% PEG200 weight fraction, respectively. (F-H) show SEM micrographs of the surface of similar samples with 7%, 20%, and 50% PEG200 weight fraction, respectively. Scale bar in F,G=10um, in H=2um.

Interestingly, it was found that spinoidal decomposition in certain material mixtures could be inhibited by the addition of single acrylate monomers. The addition of hydrophilic

monomers was investigated in case the PuSL fabricated structures needed to be encouraged to absorb more water and degrade faster. However, the addition of single-acrylate hydrophilic materials, even in very small weight fractions, prevented spindoidal decomposition and caused the resin to cure to homogenous PEG saturated gels. It is likely that this inhibition of phase separation is a function of the monomer's acrylate asymmetry, as other hydrophilic multi-acrylate monomers, such as 3-arm PEG triacrylate, rapidly cure and spinoidally decompose under UV exposure.

2.4 Poly-lactic-co-glycolic acid (PLGA)

Initial work focused on trying to develop a functional resin using PLGA. PLGA is degradable in water and displays a balanced mixture of surface and bulk erosion due to its low crystallinity/highly amorphous structure. It has been used extensively in biomedical applications, as it breaks down into lactic and glycolic acid, both of which are found in vivo and handled by the body's normal homeostatic mechanisms. It was an ideal candidate for this project, and has been used before to generate cell scaffolds meant to degrade over time and generate living tissue.

The PLGA would need to contain UV-reactive functional groups in order to act as a viable crosslinking resin. PLGA-dimethacrylate was purchased from a custom polymer supplier (CM-Tek), with a request for the lowest molecular weight possible. The resulting product had a peak Mw of 1840, and rather than being a smoothly flowing liquid was a highly viscous substance with the consistency of stiff taffy (see Fig. 2.4). This meant that the PLGA-dma would have to be dissolved in a solvent to be used in conjunction with the PuSL technique.

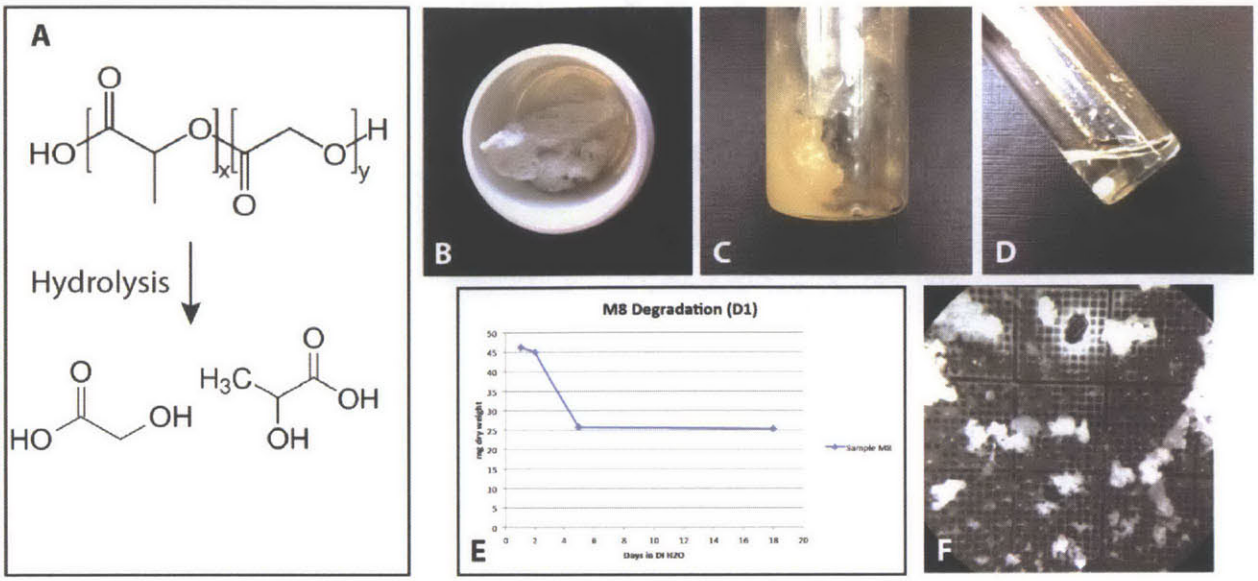

Figure 2.4: PLGA investigation. (A) Dimethacrylate PLGA would be perfect for this application, as the material degrades into lactic and glycol acid, chemicals easily handled by the body. (B) A sample of PLGAdma with Mw of ~25,000, and (C) a sample with Mw of ~1840. (D) shows (C) solvated in PEG200, 50/50 weight fraction. The solution was unacceptably viscous. (E) shows degradation of a nano-porous PLGAdma/TMPEta construct in PBS at 37C; the material lost its full weight fraction of PLGA after 6 days, and the remaining structure only contained the weight of the non-degradable TMPEta. (F) Shows grid structures fabricated with PLGA solvated in PEG200; rinsing with ethanol or water causes problematic precipitation.

Many attempts were made to solvate the PLGAdma and yield a homogenous, non-viscous solution, and various solvents cited in the literature were investigated. Dimethylformamide and N-methyl-2-pyrrolidone both solvated the PLGAdma well, creating a clear solution. However, both of these are noxious solvents that should not be used outside of a protective hood. Tetrhydrofuran (also toxic) yielded a cloudy solution, and both ethyl lactate and ethylene glycol failed to solvate the PLGA.

Ultimately, straight PEG200 was found to be the best discovered solvent for this application. It created a homogenous solution at room temperature if given sufficient time to solvate, and conveniently was found still to fulfill its role as a porogen. However, the solution was viscous, and did not flow easily through the delivery needle and tubing. Furthermore, and more problematically, the rinsing solvent to be used after fabrication had to be able to solvate

both PEG and PLGA. Fig. 2.4f shows structures fabricated with this resin that were then rinsed with ethanol, which does not solvate PLGA. As this route of investigation was sapping an undue portion of resources and time, it was deemed a lower priority until the machine was fully operational and fabrication techniques had been more thoroughly established. The development of a working PLGA resin is currently ongoing, and a supplier was recently found that offers a low-molecular weight (pipettable fluid) PLGA that might prove more promising for application.

2.5 Divinyl adipate

It became apparent that it would be advantageous to have a monomeric resin, rather than polymeric resin, that would allow hydrolytic degradation. The majority of the resins used by the Fang group were 98% monomer and 2% initiator, and such resins allow fabrication of high-resolution features and cure rapidly (after 1-3sec exposures). A fluid monomer resin would not require solvent and would likely be very low viscosity. The question, therefore, was what diacrylate or dimethacrylate monomers would phase-separate from PEG when cured, and could be used to crosslink into a hydrolytically degradable solid.

After reviewing the literature and combing through chemical supplier websites, a promising candidate was found in the form of divinyl adipate (DAP). DAP has been used as a crosslinker to create biodegradable chitosan hydrogels[27] and as a component of biodegradable thermoplastic block copolymers[28]. Although the degradation of crosslinked networks made entirely of DAP has apparently not been studied, crosslinked networks containing both DAP and hydrophilic polymers have been shown to undergo approximately 45% degradation by weight over a period of 30 days at pH 7.4[29], and the incorporation of a minimal weight fraction of slightly longer hydrophilic crosslinkers has been shown to significantly accelerate degradation[30]. It has been shown to be biocompatible, integrating well into living bone, and has been used

before as an acrylate resin for additive manufacturing[31,32]. Accordingly, DAP was deemed a promising candidate for making hydrolytically degradable structures.

DAP proved cheap to procure and is easy to work with, mixing with PEG and solvating common PEG-acrylates. It was found that a 50%DAP/50%PEG200 mixture cured into a porous solid, but the exposure times for fabrication were prohibitively long: 10um deep cure penetration, when using a standard 10pt grid pattern, required exposures of approximately 2.8-3 seconds at 100% power. It was also found, however, that the speed of crosslinking could be increased by the addition of multi-arm acrylate molecules, even in relatively small quantities. Trimethylolpropane ethoxylate triacrylate (TMPEta, Mw ~428) was found to be effective for this purpose, and an initial functional resin of 35%DAP/15%TMPEta/50%PEG200 was eventually settled on due to its excellent pore morphology and rapid cure time.

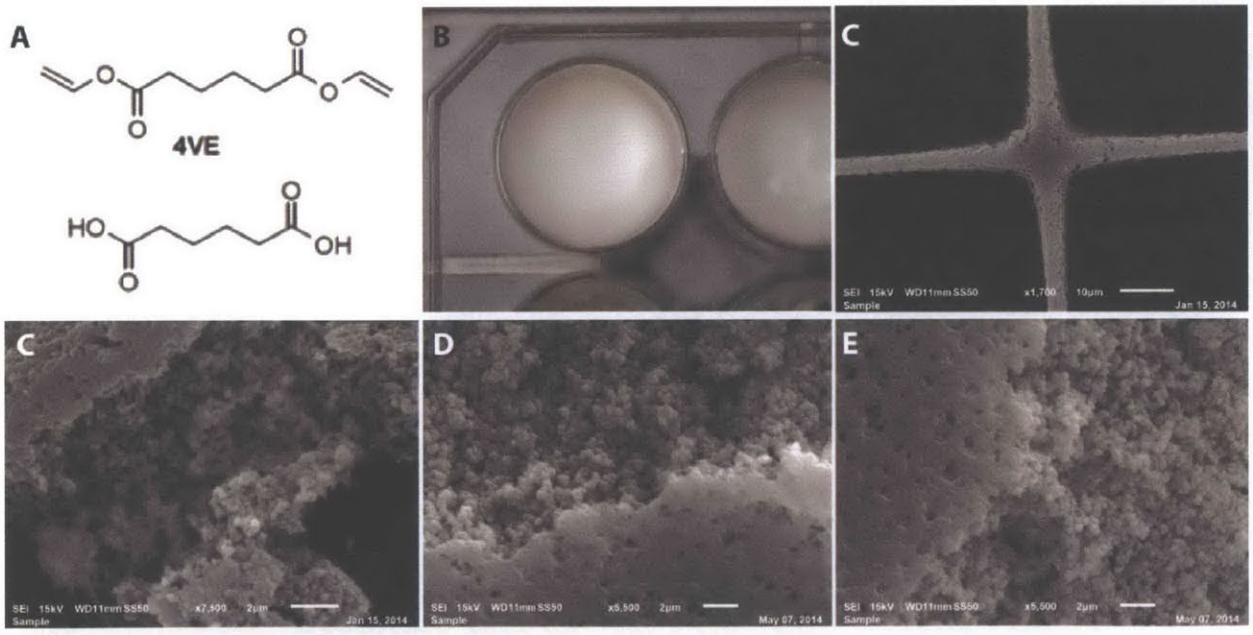

Figure 2.5: DAP investigation. (A) shows the chemical structure of DAP and the hydrolytic degradation product. (B) shows a bulk sample of DAP/PEG200 (50/50). (C) shows a detail from a grid pattern made with a DAP/TMPEta/PEG200 (35/15/50) resin; cure time was 0.7sec, scale bar is 10um. (D-E) show close-up images of fractured samples with 50%, 60%, and 70% PEG200, respectively. Both surface and interior structure of the material can be seen; scale bars are 2um.

This resin displayed good functional resolution and was used for many fabrication attempts. It should be noted, however, that the weight fraction of non-degradable material in this resin is likely high enough to prevent complete degradation, similar to that shown in Fig. 2.4. Therefore, alternative formulations are under investigation in which the 15% TMPE fraction is replaced by smaller amounts (1-2%) of other multi-arm acrylate PEGs that may similarly minimize the required cure time.

2.6 Cytotoxicity testing

When it became clear that this resin mixture would be the material of choice for many prototype scaffolds, it was important to test for any cytotoxicity. All of the resin mixtures developed for this project used a photoinitiator called Irgacure 819, or Phenylbis(2,4,6-trimethylbenzoyl)phosphine oxide, which is a free-radical generator and is not approved for biological use. Scaffolds made with this initiator were soaked in a massive excess (20ml per 5ul of scaffold volume) of 100% ethanol for 48 hours, and then rinsed in sterile PBS 3x for 1 hour. Following this washing step, a contacting and non-contacting cytotoxicity test was carried out in tandem. For the non-contacting test, scaffolds were suspended in perforated cell-culture inserts above already confluent healthy cultures of mesenchymal stem cells, and live-dead staining was performed following 24-hours of incubation. For the contacting test, scaffolds were fabricated similar to those discussed in section 3.6 and seeded with iPS-derived endothelium and cultured for three days. Neither of these assays showed cell death greater than control conditions, and the 35DAP/15TMPEta/50PEG resin displayed excellent cell attachment, likely due to the material nanostructure.

2.7 Using dye to control cure depth and reaction propagation

The foremost obstacle to reliable microfabrication using PuSL is maintaining control over cure depth and width. These parameters are affected by the inherent reactivity of a given material, and can be moderated by the presence of photo-absorbing agents such as the common lipophilic dyes Sudan I and Sudan 7B. Without any dye concentration, some of the more reactive materials used were found to cure ~50 um deep when exposed by a10px wide line, and ~250um deep when exposed over a broad (1080px full white) area. Much effort has gone into determining functional minimum concentration of these dyes.

Unfortunately, development on this front has been hindered by the tendency for the lipophilic small-molecule dye to absorb into the PDMS print-window (Fig 2.6a). To achieve high-resolution fabrication, the Fang group, which printed on a free-fluid surface, used dye concentrations of up to 0.75%. In our system, using 100% PEG or HDDA, this dye concentration limited the penetration depth to approximately 20um (Fig. 2.6d). However, this concentration of dye also stained the PDMS so severely it began affecting cure times, which was unacceptable for lengthy builds. As I was attempting to achieve even smaller cure depths on the order of 1-5um, it was clear that a substitute for either the PDMS or Sudan I would need to be investigated.

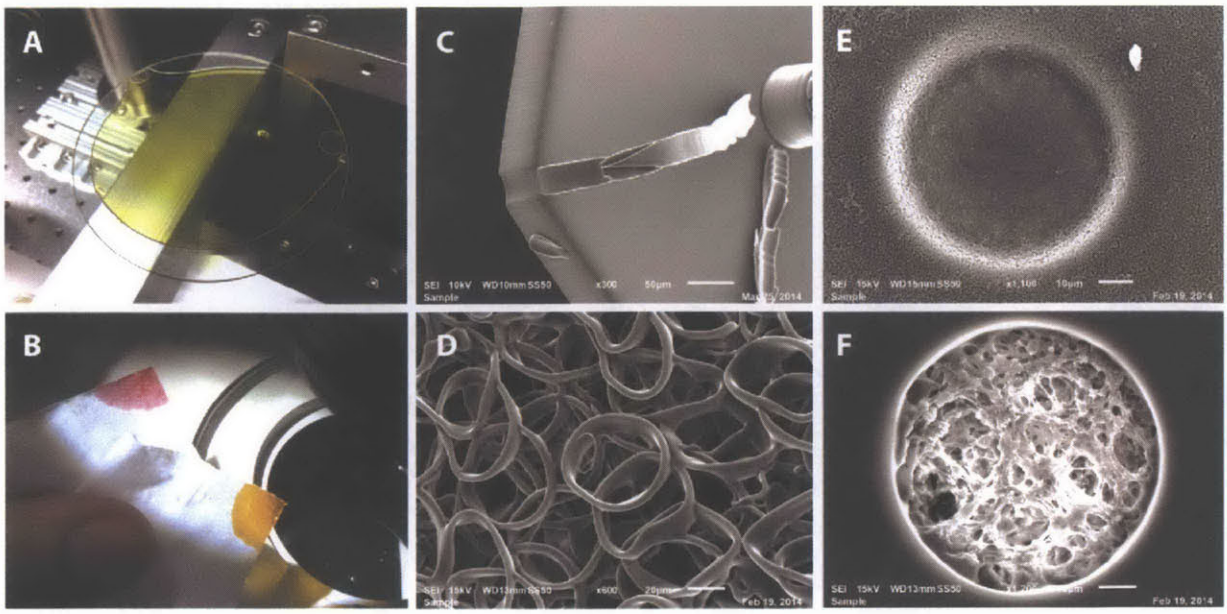

Figure 2.6: Photoabsorber investigation. (A) Lipophilic dyes were found to stain the PDMS in the top window. (B) Image showing the colors of solutions of Sudan I (orange) and Sudan 7B (red-pink). (C vs. D) shows the effect of dye concentration on cure depth; (C) used a resin with 0.05% S1 and displayed a cure depth of over 50um, (D) used a resin with 0.75% S1 and showed a cure depth of ~20um. Dye concentration also affects XY feature definition: (E) was made with a resin with no dye; negative features over 50 um in diameter were completely occluded, (F) was made with the same resin used in (D), and shows almost no negative feature occlusion.

Sudan I has two absorption peaks, one at 418nm and one at 476nm, meaning that it absorbs blue light and appears orange. This made it a good contender for stereolithography work using visible-range UV light, around 400nm. A molecular cousin, Sudan 7B, has an absorption peak at 364nm, nearly identical to the UV light produced by the LED in our system. It was hoped that a combination of these two dyes could be used to create a broad UV damping effect that might allow a reduction in cure depth while simultaneously reducing staining of the window.

This work is ongoing. Both dyes were found to stain the PDMS, though Sudan 7B does less so than Sudan I. Options are being investigated for a) replacing the PDMS with another, less lipophilic material, and b) potentially replacing the Sudan dyes with other UV absorbing components that might not integrate into the PDMS.

Conclusions and future directions

The power of the PuSL technique is amplified by its ability to work with a very broad range of materials. Any non-viscous solution with acrylate, metharcrylate, or similarly UV reactive crosslinking functional groups is theoretically capable of being cured using PuSL. This opens up the possibility of building with synthetic polymers (such as PLGA), synthetic monomers (such as DAP) and even biological molecules, such as acrylated collagen, hyaluronic acid, and other polymeric ECM proteins. The flexibility of the fabrication system, and the reliability with which multi-acrylate materials form nanopores when cured as a mixture with PEG200, means that resin options and development is open-ended, and further functionality can likely be built into future materials with minimal difficulty.

The primary resin-development goals were met by DAP-based solutions. These resins are low viscosity, cure small features in about 0.5 seconds, are non-toxic, phase separate into a nano-porous solid that roughly mimics native ECM, and yield structures with satisfactory cell attachment. The degree of degradation remains to be investigated. Although this resin has been used before to generate degradable scaffolds, it was always in combination with other crosslinking monomers, and the degradation times were quite long, on the order of many months. Tuning DAP resins to yield structures degradable on shorter time spans may require additional chemical modification.

Chapter 3: Development of operational techniques, experimental methods, and functional scaffold designs

Introduction

Following completion of the PuSL apparatus, attention shifted to finding ways to work with various materials and developing protocols for generating microfabricated parts. This work was completed in tandem with the work discussed in Chaper 2, and as such, certain fabrication experiments were carried out with non-optimal resins. Nevertheless, important pieces of information have been learned regarding the strengths and weaknesses of this fabrication technique, as well as what challenges lie ahead for this research to fully achieve its aims.

Learning how to use this piece of equipment to effectively fabricate has been an iterative process. The machine itself contains no programming architecture or automation, so any task with multiple steps requires a specialized code to be written in advance. Additionally, it was found that a single fabrication code would not work for all scaffold designs, so the development of a new scaffold type generally required the writing of a new LabView code structured to work in tandem with a given class of scaffold. These demands lead to a cyclic process of designing a scaffold, writing a code to build it, validating the code, fabricating the part, and then learning how that part must be redesigned to be effectively fabricated – effectively starting the process over.

Assessment of built scaffolds was generally carried out by a combination of stereo light microscopy, transmission light microscopy, and scanning electron microscopy. Each of these techniques yields information that the others cannot provide. Stereo light microscopy is excellent for immediate assessment of scaffolds, as it produces a 3D view, and can image

scaffolds without dehydration. Transmission microscopy shows material density, and can be used to assess the local degree of material cure. SEM is the most revealing technique, but it is also limited in that it requires drying of the samples, which can make assessment of certain features difficult, particularly if the scaffolds buckle, fracture, or contract during drying.

This chapter details four main classes of scaffolds that have been pursued: a) single image rectangular arrays, b) multi-image stitched arrays, c) duplicate Z-stack hexagonal arrays, and d) dual-lens constructs. The hexagonal array code and class of scaffold has proved the most relevant for application to liver tissue engineering, and encompasses three sections detailing scaffolds with increasing complexity: vertical vasculature scaffolds, scaffolds for vasculogenesis, and scaffolds with branching microvasculature.

3.1 Operation overview

The fabrication of a scaffold starts one of two ways. If the desired end product is a vertical extrusion (i.e. every Z-slice will be the same and there are no overhanging structures) then a standard vector-based drawing program such as Adobe Illustrator can be used to draw the cross-section to be printed. This route is advantageous in that scaling is readily calculated between the drawn part and the resulting product: the units used on-screen are pixels, which are represented exactly on the DMD chip. If the desired end-product is not a simple vertical extrusion, however, then the model must be drawn with a 3D CAD program such as Solidworks, Rhinonceros, or AutoCad. This 3D model is then exported to an STL file, with resolution settings calibrated to yield a smoothly-surfaced part for the chosen units. This STL file is then exported to 3D slicing program (Netfabb was used for this project) and sliced at regular intervals to yield a set of bitmap (BMP) files, each of which represents a cross-section of the part at a given elevation.

Once these files are obtained, a series of manual steps must be completed in order to prepare the machine for fabrication. Constructs can be built on either glass coverslips or PVDF filters. While the filter is easiest to work with, glass coverslips allow analysis of resulting structures using optical transmission microscopy. For both substrate types, it is crucial that the substrate be anchored to the piston prior to fabrication and that the starting fabrication height be aligned within approximately 20um of the print plane. If fabrication is begun with the piston below this elevation and the 10:1 reduction lens is used, the resin will not cure deeply enough to anchor to the substrate. Once the substrate is attached to the piston and at the correct level, the PDMS/quartz glass window is clamped onto the print plane, and the appropriate lens swung into alignment and fastened in place. A starting layer of material is then injected into the chamber, and fabrication can begin.

The number of modifiable fabrication variables in this apparatus is extensive. Table 3.1 shows the effect of modulation of various build parameters; as the effect of certain parameters overlap with others, many problems can be tackled from multiple directions.

Table 3.1: Relevant fabrication variables

Category	**Parameter**	**Impact on fabrication**
Light source	Exposure time*	Impacts degree of cure Impacts speed of cure Impacts depth of cure (Z) Impacts horizontal extent of cure (XY)
	Power*	Same as above; both impact effective light dosage
	Focus/alignment	Impacts Intensity Impacts evenness of cure across exposure plane
Stages	XY distance*	Impacts stitching of exposures
	XY speed / code timing	Code specific Creates "streaked" features if not properly adjusted
	Initial Z height*	Too high: no cure due to oxygen gradient, glass slide with suction to PDMS Too low: cured material will not attach to

		substrate
	Z step-size*	Driven by solid model Impact on horizontal extent of cure (XY)
	Z speed	Fast speeds can tear fabricated layers due to fluid shear
Image	White/black levels	Modulates light intensity (white level), and feature definition (contrast) Grayscale gradient masks can be used to compensate for light intensity gradient
	Linear size of solid model features in slice image	High impact on cure depth High impact on cure time
	Arrangement of features in slice image	Relates to above; closely spaced features effectively amplify local intensity due to point spread
	Size of image	Affects scale and subsequent feature size
Material	Dye content	High impact on cure depth (Z) Impact on cure extent (XY) Low impact on cure time
	Inherent reactivity	Impact on cure depth (Z) Impact on cure time Impact on cure extent (XY) Impact on potential resolution
Substrate	Position and attachment*	Impacts long-range structure variation (diffusion gradients) Impacts potential Z-speed
	Character*	Impacts potential materials to be used Impacts initial Z height

**Indicates that a parameter is material dependent. Optimal values must be determined for each resin used.*

3.2 Point spread and thresholding in PuSL

Fabrication with PuSL is governed by the point-spread function of the apparatus used. The point-spread function, or PSF, is a fundamental concept in optical engineering, describing the response of an optical system to single point of light of arbitrary intensity. In a PuSLA, the PSF is a function of both the light source and the optics. Figure 3.1 shows the basic principles of the PSF for basic projection onto a surface.

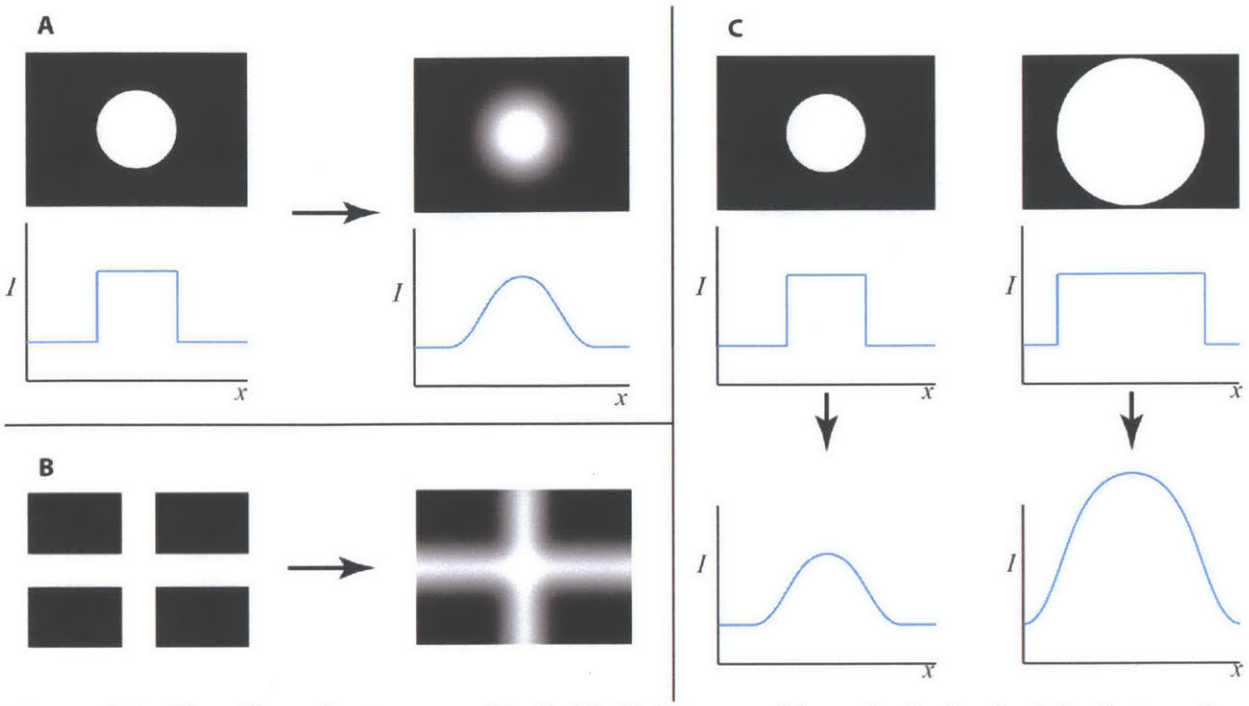

Figure 3.1: The effect of point spread in PuSL. Point-spread is a physical principle that can be minimized but not overcome. Single points of light, represented by an input step-function, are blurred during projection, and are output at the print-plane as a Gaussian intensity distribution (A). This has relevant effects on feature definition, as it means that corners and edges will become rounded (B). Additionally, features with broader cross-sectional distance will generate areas of higher mean intensity (C), and as intensity correlates with cure depth, will consequently generate deeper features. Excellent references for techniques to quantify these effects in PuSL are Sun et al. and Itoga et al.[24,33]

There are three immediate consequences of point-spread. 1) As all features are slightly blurred, hard corners cannot be achieved. 2) The feature size yielded for a given pattern depends on light intensity. Increased intensity creates a broader light distribution, widening exposure area in the XY directions. 3) Broader features yield deeper cure depths, as point-spreads add over an area, and increased intensity correlates to deeper cure.

In addition to the PSF, fabrication with PuSL has to take into account material-cure effects. Figure 3.2 shows that the spacing of even-sized features can affect feature definition. The point-spreads from all features are additive, and if features are sufficiently close together, they will not only increase the intensity of each apex, but also create a field of non-zero light

intensity between them. If the resin in use has an optimized cure-threshold (t_2 in the image), features approximating the input function can be generated. However, if the cure-threshold is too low (t_1) negative features will be occluded and if the cure-threshold is too high (t_3), then no material will cure. The reactivity of the material to UV light consequently has an impact on the efficacy of a given fabrication protocol. Material reactivity has been found to be a function of initiator concentration, inhibitor concentration, photo-absorber concentration, solvent concentration, and the molecular structure of the reactive species.

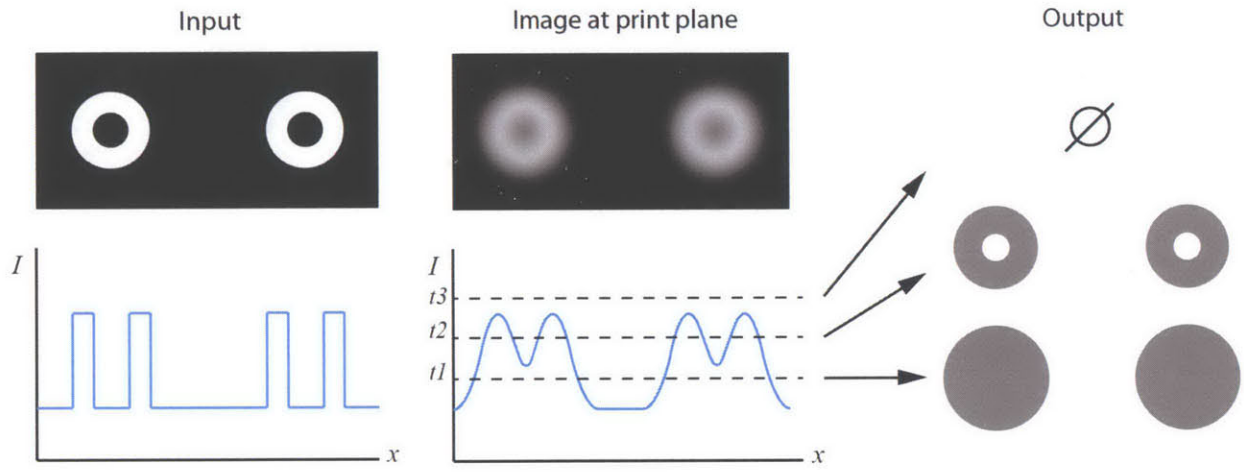

Figure 3.2: Thresholding. Due to point spread in complex patterns, feature spacing, feature cross-sectional area, and resin reactivity all interact. t1, t2, and t3 represent cure thresholds for different resin mixtures. The resin reactivity can determine whether a given set of experimental parameters used with a given projection yields proper features, no features, or over-cured features. Likewise, different designs can yield different feature definitions even if the resin and experimental parameters are held constant.

3.3 Vertical fabrication

The first three-dimensional build code was designed to print a three-axis array of a single image at a given spacing in each dimension. Fabrication codes generally took the form of single-run state machines with highly nested FOR loops and stacked sequence structures. This code was designed to operate in the fashion of a three-dimensional typewriter: printing a row X exposures long, returning to the start point, and moving down a row width, doing this complete

cycle Y times, then returning to the origin, moving down a Z increment, and performing the entire planar operation once again until the desired number of layers had been completed. For this code, all exposures were of the same image, and the pattern was usually generated as a 2D drawing.

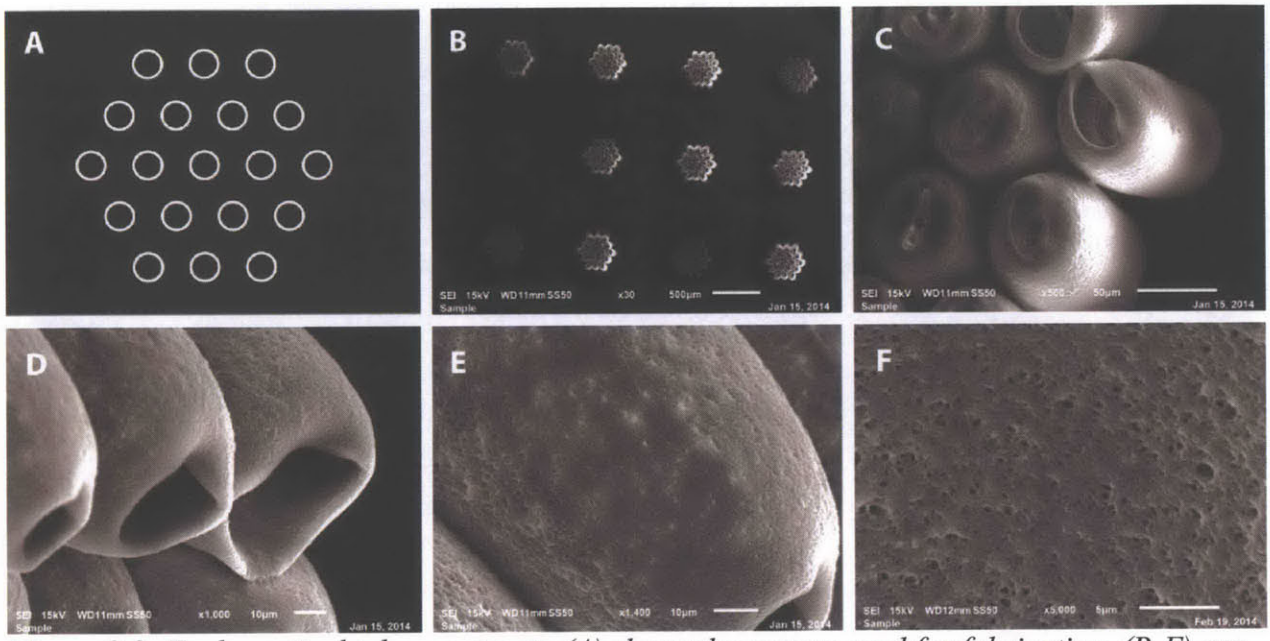

Figure 3.3: Early vertical tube constructs. (A) shows the pattern used for fabrication. (B-F) are SEM micrographs of the fabricated tubes. Note the hollow lumens in (C) and (D) and the nanoporous character in (E) and (F). Parts shown were built using 35%DAP/15%TMPEta/50%PEG200/2% Irgacure 819, with no dye added.

An early case study is presented in Fig 3.3. This experiment was performed with an early-used resin mixture of 35%DAP/15%TMPE/50%PEG200 containing no dye; as such, the fabricated features are not precise. The three-dimensional extruded tubes were made using the pattern in 3.3a; this pattern was exposed in a 3x4 grid with a spacing of 1mm, for 10 layers with a step size of 20um. These were the first demonstration of patent tubes made using the PuSL with a degradable porous resin. They were too large to act as microvasculature (approximately 50um in internal diameter), but nonetheless were an encouraging preliminary result.

3.4 Rectangular multi-image stitched arrays

Although the 10:1 reduction lens boasts excellent feature resolution, the effective print area is only 740um to a side. This means that to use this lens to build a larger construct with features that repeat on length scale greater than 740um, the X and Y stages must move while Z remains fixed, and multiple exposures must be laid down with their edges touching to generate a single vertical cross-section of the part. Each Z-layer, instead of involving a single projected image, is therefore made up of multiple smaller bitmap images, exposed one at a time.

This necessitates both an extra step for image-processing (slicing vertical cross-section images into an X by Y grid of smaller tiles), and a more complicated piece of code, as each new exposure has to draw on a new image file. A code was designed to draw from an input folder file, printing each image sequentially. For instance, if each Z-slice were to be made from a 12x12 grid of images, the code would sequentially print "scaffold_01_01" through "scaffold_01_144" and then move down a layer and print "scaffold_02_01" through "scaffold_02_144," etc. This method of fabrication accordingly requires a large amount of storage space, as a single part may pull from 2000-3000 distinct image files.

At the onset of this thesis, it was thought that this technique would be a catch-all, allowing the fabrication of basically any design with relative ease following proper image slicing. However, it was found that stitching of exposures was very difficult to properly calibrate. Though lateral exposure stitching had been demonstrated successfully by the Fang group, the designs they employed allowed attachment of broad features that were forgiving of slight misalignments. Stage movement was not the problem – our stages could accurately place the exposure within 250nm of the desired location – but rather that slight differences in cure time or image pattern would cause differences in the extent of lateral XY cure. This meant that unless

features were built into the design to allow overlap, variation in the pattern on a given image tile could mean the difference between successful stitching or a macroscopic part with little mechanical integrity.

Fig 3.4 shows an example of a successfully stitched part. The ultimate conclusion was that this technique was possible, but likely not worth perfecting. Macroscopic parts with large positive and negative features were found to be easier to fabricate with the 1:1 lens, and smaller features, particularly for a tissue such as the liver, could be pattered to align with the spacing of a single exposure and thus not necessitate arbitrary part slicing and stitching.

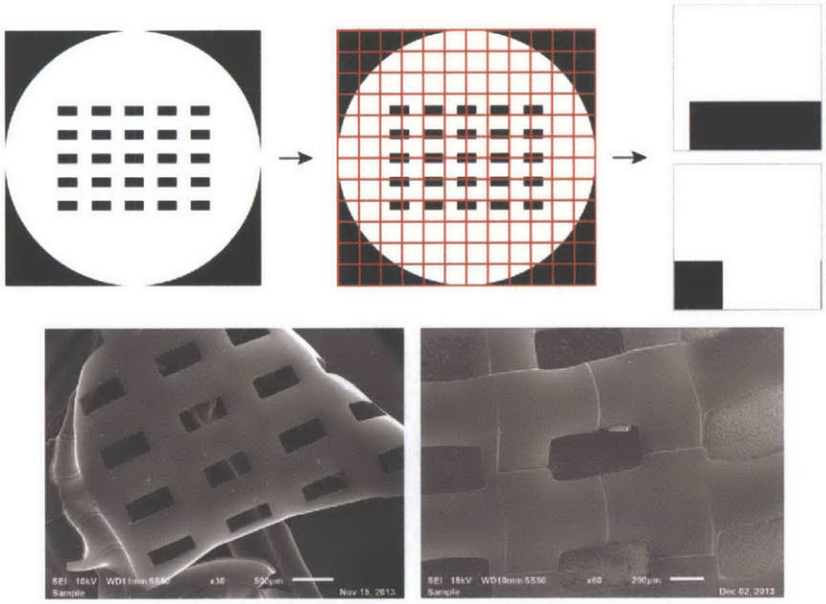

Figure 3.4: Rectangular stitching process and result. This technique was effective but difficult to calibrate. Additionally, it proved a slow way to fabricate parts with large features, and the 1:1 lens was found to be better suited to the task. Parts shown here were fabricated from 98%HDDA/2%Irgacure819 with 0.05% Sudan I.

3.5 Hexagonal stitched arrays

It was clear from the above findings that fabrication would be most reliable if the scaffolds to be generated displayed a repeating structure with a periodicity equal to the exposure size. This was convenient, given that the maximum exposure size (vertical dimension) was 740-750um, and native liver histology shows a lobule periodicity of 600-800um. Simple hexagonal

liver lobule scaffold designs were subsequently drawn with an inscribed circle diameter distance of 750um, examples of which are shown in Fig. 3.5a and Fig. 3.5c.

A separate LabView code had to be written for this method of fabrication as well. The module was written so that the hexagon size could be input and the code would calculate the exposure spacing in both dimensions, and was designed to print an oscillating "grid" of close-packed hexagon exposures with X rows and Y columns, as can be seen in Fig. 3.5d. This code is a hybrid of the earlier two fabrication codes: the final part must periodically repeat on the XY axis, but can print a different image for each Z-layer, effectively creating a set of repeating units, each of which in isolation can have unconstrained complex architecture.

This method of fabrication proved the most powerful and applicable to liver engineering. Fabrication with this technique is shown in Fig. 3.5d-3.5i. Two conclusions can be taken from these images. First, fabrication in this format is effective and repeatable – the broad edges of the hexagons provide good opportunity for exposure stitching, and robust parts are yielded that resemble the solid model. Second, small scale features such as vascular structures must be placed inward from the edges/corners – the SEM images in 3.5f show that stitching of features with small cross-sectional area is difficult to achieve. Future scaffolds were therefore designed with whole tubes (rather than 1/3 sections) at each corner, which when arrayed appear similar to a portal triad in the liver (see Fig. 3.5i).

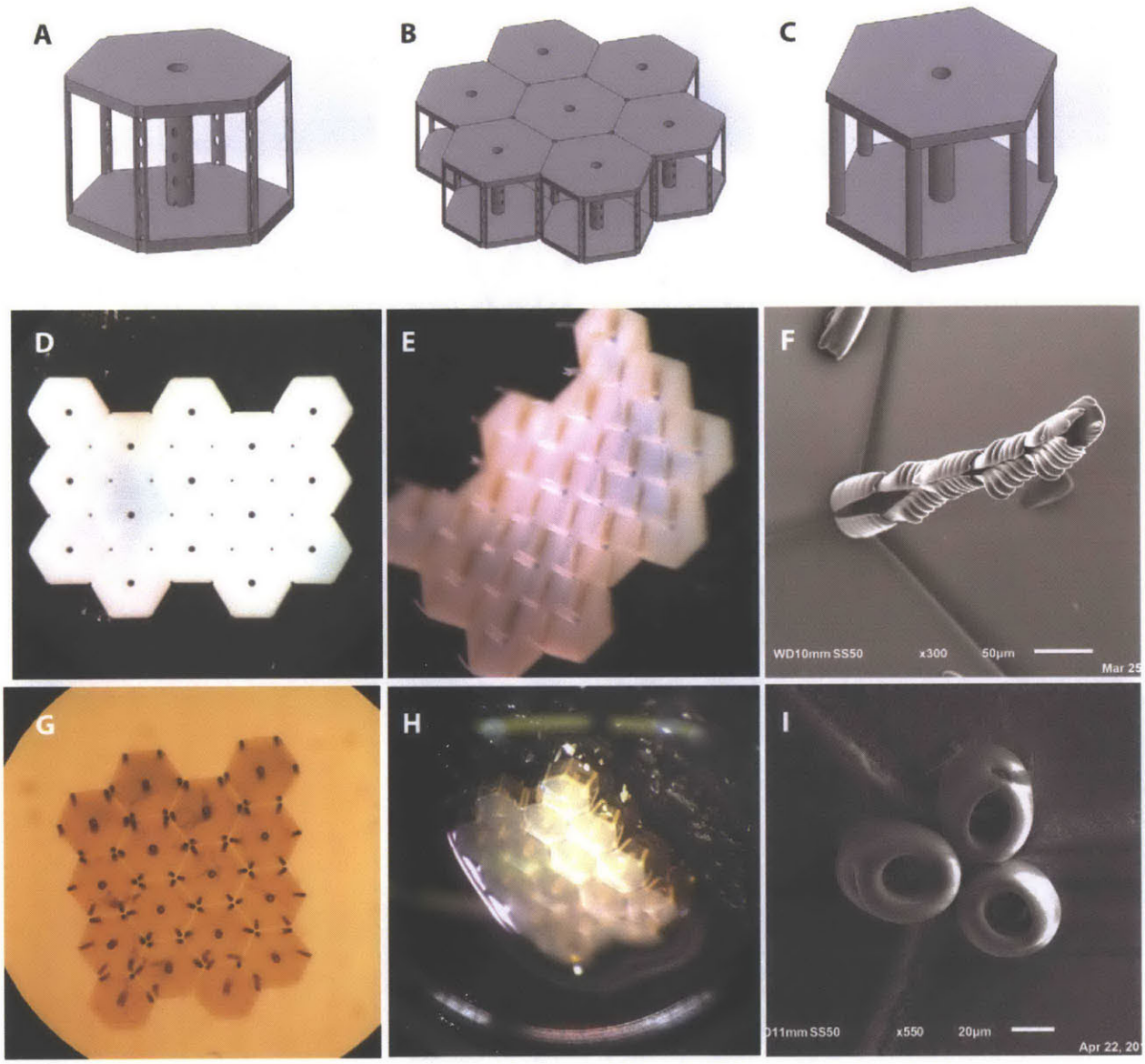

Figure 3.5: Hexagonal array fabrication. (A-C) show various solid models intended for fabrication with this technique. (D-F) are images of structures built using the design shown in (A), in which each corner was meant to construct one third of a small tube. (G-H) shows structures built using the design shown in (C) which ultimately proved more successful. Note the precise exposure stitching in (G), high aspect ratio tubes in (H) and patent lumens in (I). These scaffolds were built using 35%DAP/15%TMPEta/50%PEG200/2% Irgacure819, with the exception of (F), which was made with 98%HDDA/2% Irgacure819. (D) contains no dye, (E-I) contain 0.05% Sudan I and 0.1% Sudan 7B.

3.6 Vertical tubes with openings for capillary branching

It has been a longstanding discussion in the world of tissue engineering and regenerative medicine as to whether or not it is even reasonable to fabricate functional capillary networks. Although it may be possible to process materials on a small enough scale to achieve complex branching fluidic networks, it is likely difficult to design a three-dimensional network that will generate physiologic gradients of nutrients and relevant cell-morphology guiding signals. It is desirable, therefore, to develop constructs whose architecture allows and encourages cell-directed vasculogenesis.[34,35]

Fig. 3.6 shows a design for a liver scaffold intended to allow this process; some scaffolds shown in Fig 3.5 were designed toward this aim as well. These were the first designs intended for fabrication that required micron-scale overhangs. As such, the success of these builds was dependent on mixing sufficient photo-absorber into the resin to prevent the occlusion of fabricated openings by higher-elevation exposures. As discussed in Chapter 2.7, the absorption of dye into the PDMS print-window generally hindered this aim. The ellipsoid shape (20umx40um diameter) of the capillary openings was designed to allow fabrication with lower dye concentrations, as small holes would still be available for vascular branching even if fully accurate fabrication could not be achieved. Various fabrication results can be seen in Fig. 3.6c-3.6f. This design was deemed successful, and will be tried in the bioreactors along with various cell combinations.

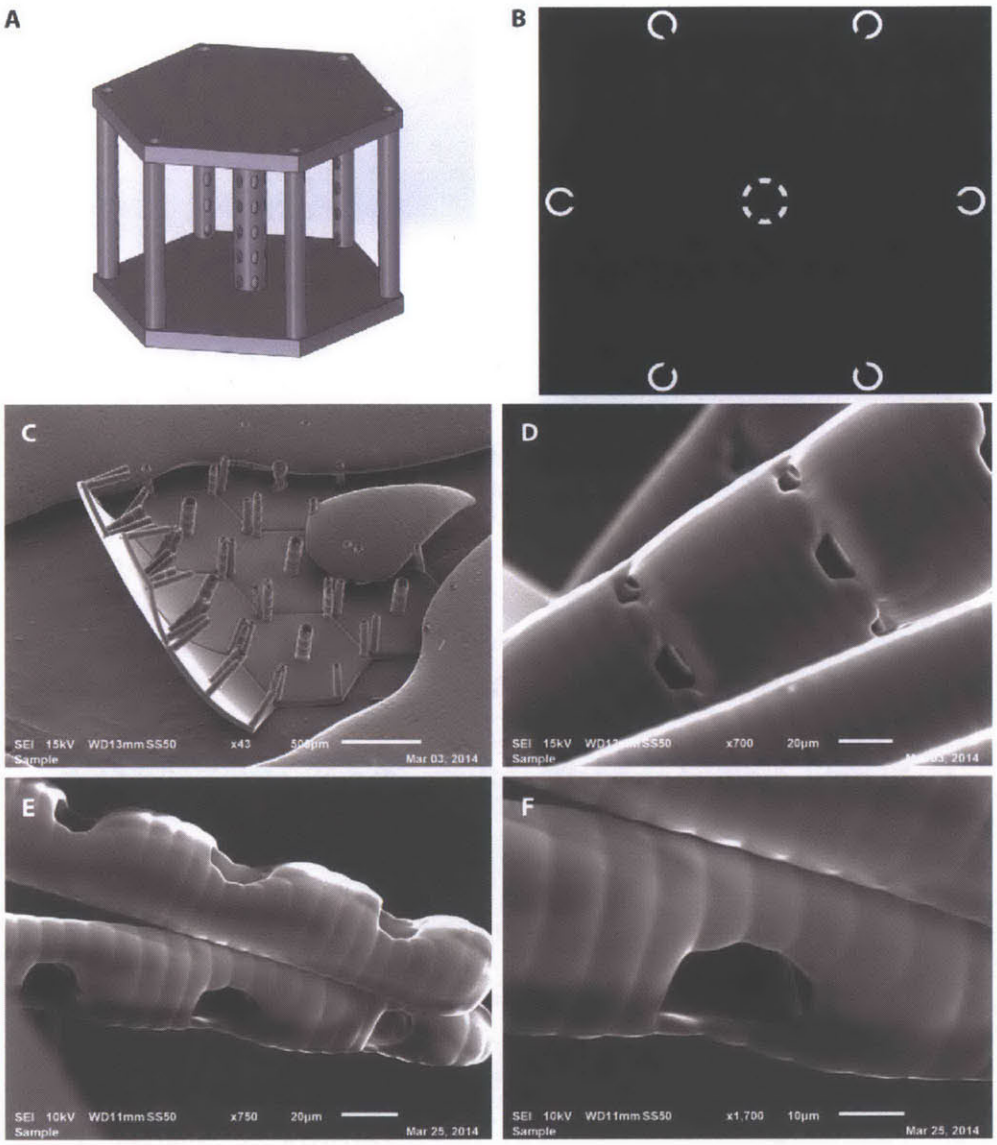

Figure 3.6: Scaffolds with holes for capillary formation. (A) shows the solid model used. (B) shows a single cross section at the central elevation of the overhanging holes. (C) shows a stitched array using this design. Successful fabrication depended on dye concentration, as high cure depths would occlude the hole openings (D). Resins with sufficient dye can be used to make 40um diameter arterioles with ~10um diameter openings that might act as starting points for a flow-motivated self-assembled endothelial microvascular network. All scaffolds shown here made with 98%HDDA/2% Irgacure 819. (C,D) used 0.05% Sudan I, 0.01% Sudan 7B. (E,F) used 0.05% Sudan I, 0.1% Sudan 7B.

3.7 Dual lens constructs

Liver projects in the Griffith laboratory were known to require scaffolds with small areas of high-resolution construction held together by larger features. The ability to expose patterns

with the 1:1 lens would, in theory, shorten build times, and allow the generation of macroscopic, low resolution features without requiring lengthy stitched-exposure processing using the 10:1 reducing lens.

Generation of ~50um positive and negative features has been demonstrated using the 1:1 lens, and though the exposure light intensity is more than 10-fold lower than with the reducing lens, it has proved capable of curing all materials investigated if given sufficient time (some exposures need to be on the order of 5 minutes). This lens is being used currently to generate macroscopic hydrogel-based scaffolds similar to those shown in Fig. i.2b.

Fabrication using both the 10:1 and 1:1 lenses in conjunction presents a number of challenges. Lens switching involves a manual operation of swinging the lens against a hard-stop and then clamping it in place. This was found to demonstrate a linear repeatability for the 1:1 lens of approximately 250um, and of >500um for the 1:1 lens, which has a slightly different mounting structure. This means that sequential prints cannot generally be made to align well if a lens is unclamped between exposures, even if the same lens is used. Second, the intensity of the light generated by each lens differs by about an order of magnitude, which affects how far below the print plane the resin begins to cure. While the 10:1 lens can cure materials with the substrate a few microns below the print-plane, the 1:1 lens only shows visible cure once the substrate has been lowered beyond 80-100um. Since the difference in elevation is larger than the depth of most 10:1 exposures, it can be difficult to vertically stitch 10:1 exposures onto 1:1 exposures without careful Z-compensation.

These challenges were overcome by a) designing scaffolds with overlap between 10:1 and 1:1 exposure areas, so that lens alignment could be flexible without consequence, b)

segregating 10:1 and 1:1 sequences, and c) printing 1:1 exposures after all 10:1 work was completed, which took advantage of the deeper focal plane on the 1:1 lens.

Successful applications of dual-lens construction are shown in Fig. 3.7. In 3.7a, c, and e, small 1.5mm microwells were designed to capture droplets of endothelial cells suspended in a vasculogenic gel, the idea being that the 40um tall, 50um diameter starter-tubes would then concentrate the bioreactor driven perfusion flow, generating localized shear patterns that would cause the endothelial cells to align into tubes and form a vascular tree.

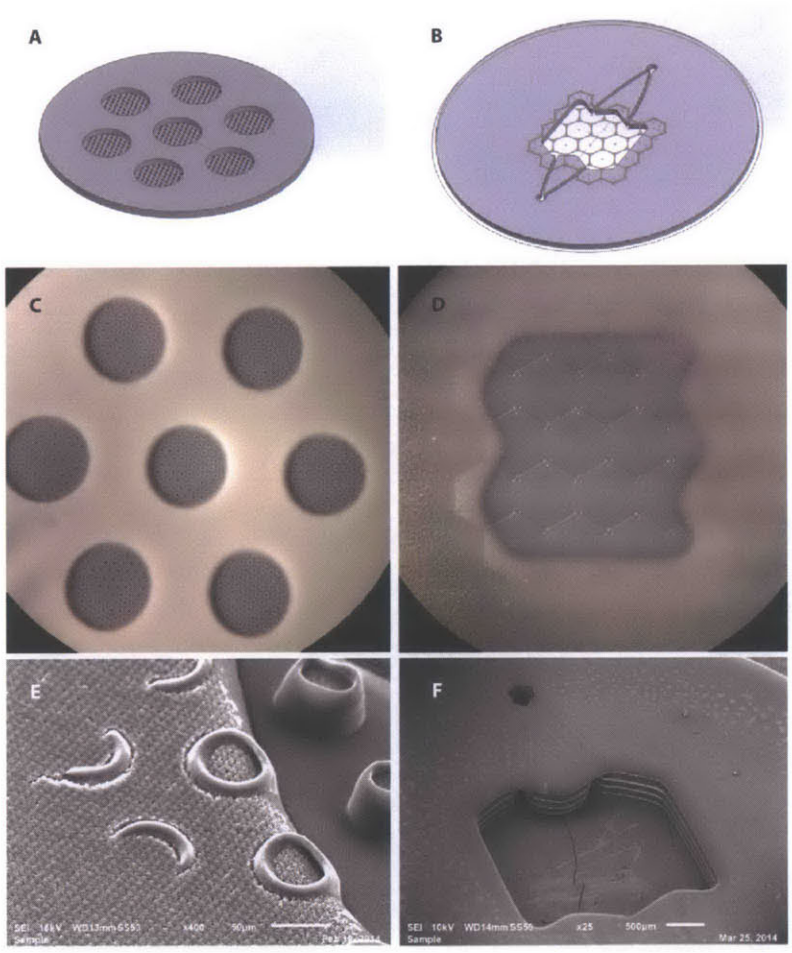

Figure 3.7: Dual-lens constructs. (A-B) show solid models designed to accommodate low precision lens-alignment. (C-D) are light microscope images of resulting builds. (E-F) are SEM micrographs of similar structures. Note in (E) the >10-fold difference in resolution between the two lenses. The cure depth of a single exposure with the 1:1 lens fully occludes smaller tubes made in four 10um deep layers by the 10:1 lens. The dimples in the texture of the 1:1 surface correspond to DMD pixels. These scaffolds were built using

35%DAP/15%TMPEta/50%PEG200, mixed with 2% Irgacure 819. Resin for images (D) and (F) included 0.1% Sudan I and 0.1% Sudan 7B.

3.8 Branching vasculature

One of the ultimate goals of this project was to make scaffolds with three-dimensional branching vasculature with physiologic scaling. The achievement of this aim is challenging, as it requires not only carefully planned scaffold designs, but also the right fabrication parameters to achieve tiny feature sizes in all three dimensions. While the earlier discussed constructs had flexibility regarding cure depth and horizontal cure extent, high-resolution thin-walled branching fluidics will not work unless they are fabricated with a high degree of fidelity to their CAD model and are able to avoid both tube occlusion and mechanical failure. This demand necessitates careful scaffold design and tight control of experimental parameters to minimize feature resolution.

A recent branching vasculature scaffold designs is detailed in Figure 3.8. Horizontal tubes like those shown in Figure 1.4b were abandoned, since, when sliced, such models generate variable 2D feature sizes and consequently have variable cure depth. Instead, models were adopted with tubes oriented at various degrees of inclination, which yield relatively even-wall thickness ellipses when sliced. The curvilinear character of these models was developed to create slices with uniform ellipses and to reduce the distance between nearest capillaries in all three axes.

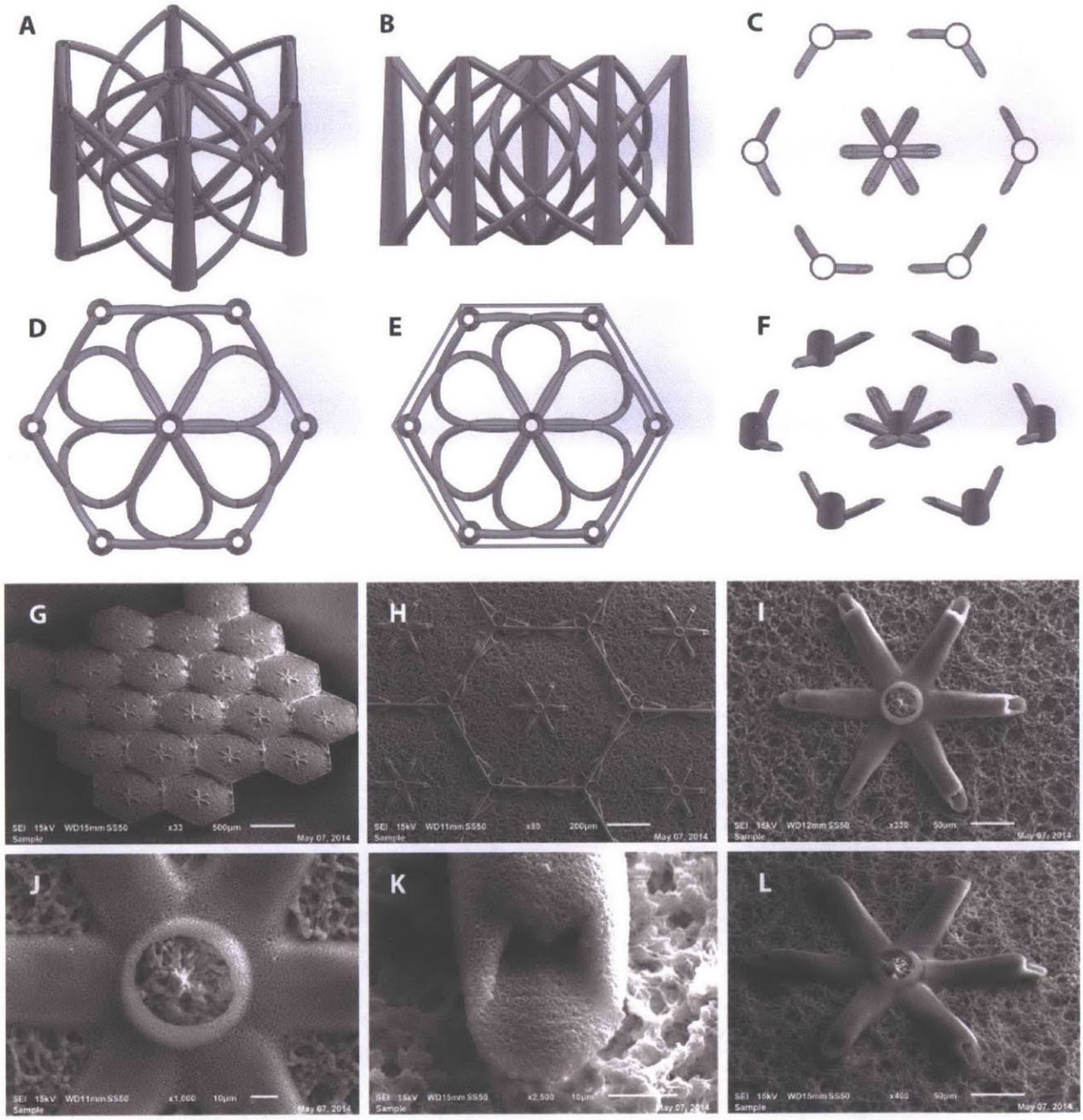

Figure 3.8: Branching vascular fabrication. (A-F) show views of a solid model used for this fabrication technique; the three dimensional curvature of the capillaries makes fabrication easier and minimizes dead space in the scaffold. (E) shows reinforcing walls, which helped to give the constructs mechanical integrity. (C, F) show two views of the scaffold truncated at 80um, reflecting the layer number and size used to build the structures shown in (G-L). Note the precise stitching in (G-H) and the fine resolution in (J-K). 45 degree observation (K-L) showed that the lumens of these structures were occluded due to ~20um resin cure depth. These scaffolds were built using 35%DAP/15%TMPEta/50%PEG200, mixed with 2% Irgacure 819, 0.2% Sudan I, and 0.25% Sudan 7B.

Following fabrication attempts with this design, two capillary-scale specific challenges became clear:

1) High levels of photo absorber are required to reduce the cure depth to a 1-3um range, critical for successful fabrication of complex scaffolds with off-axis oriented tubes with 10-20um internal diameters. There are no published precedents for fabricating with such a small vertical resolution using PuSL.

2) The point-spread function of the apparatus becomes increasingly relevant when scaffolds are designed with small feature sizes, as the thresholding effect can dominate. Within a single exposure, clustered features will cure while spatially isolated features do not cure, even if features display similar cross-sectional distances. The scaffolds therefore have to be designed and iteratively reworked with this principle in mind, making sure that isolated or thin cross-sections are "helped" in some way.

Following from these observations, scaffolds were designed with a greater density of capillaries and with columnar features next to areas of thin linear cross-section, both of which act to minimize the consequences of point-spread thresholding. Such designs can be seen in Figure 3.9; the high density of capillaries has the added benefit of mechanically reinforcing the fabricated structure and further reducing the distance over which nutrient and gas diffusion will be necessary during cell culture. By using more powerful photo absorbers to reduce the cure depth to 1-2um, ongoing experiments are close to discovering the proper protocol to fabricate such structures with high accuracy.

Figure 3.9 (on next page): Iterative vascular construction: (A-F) show views of a model similar to that described in Fig. 3.8, but with additional vascularity on multiple inclination angles and modification to counteract the threshold effect. Optical microscopy images are shown in (G-I), SEM micrographs in (J-O). Note the columns of solid material in (B, C, M, and O), added to allow construction of the corner arteries. The dye concentration used in this experiment was still not high enough to prevent capillary occlusion, as can be seen in (M-O). The XY spatial resolution, however, is quite good, allowing generation of features only a few microns wide. Further resin optimization is ongoing. These scaffolds were built using 35%DAP/15%TMPEta/50%PEG200, mixed with 2% Irgacure 819, 0.2% Sudan I, and 0.25% Sudan 7B.

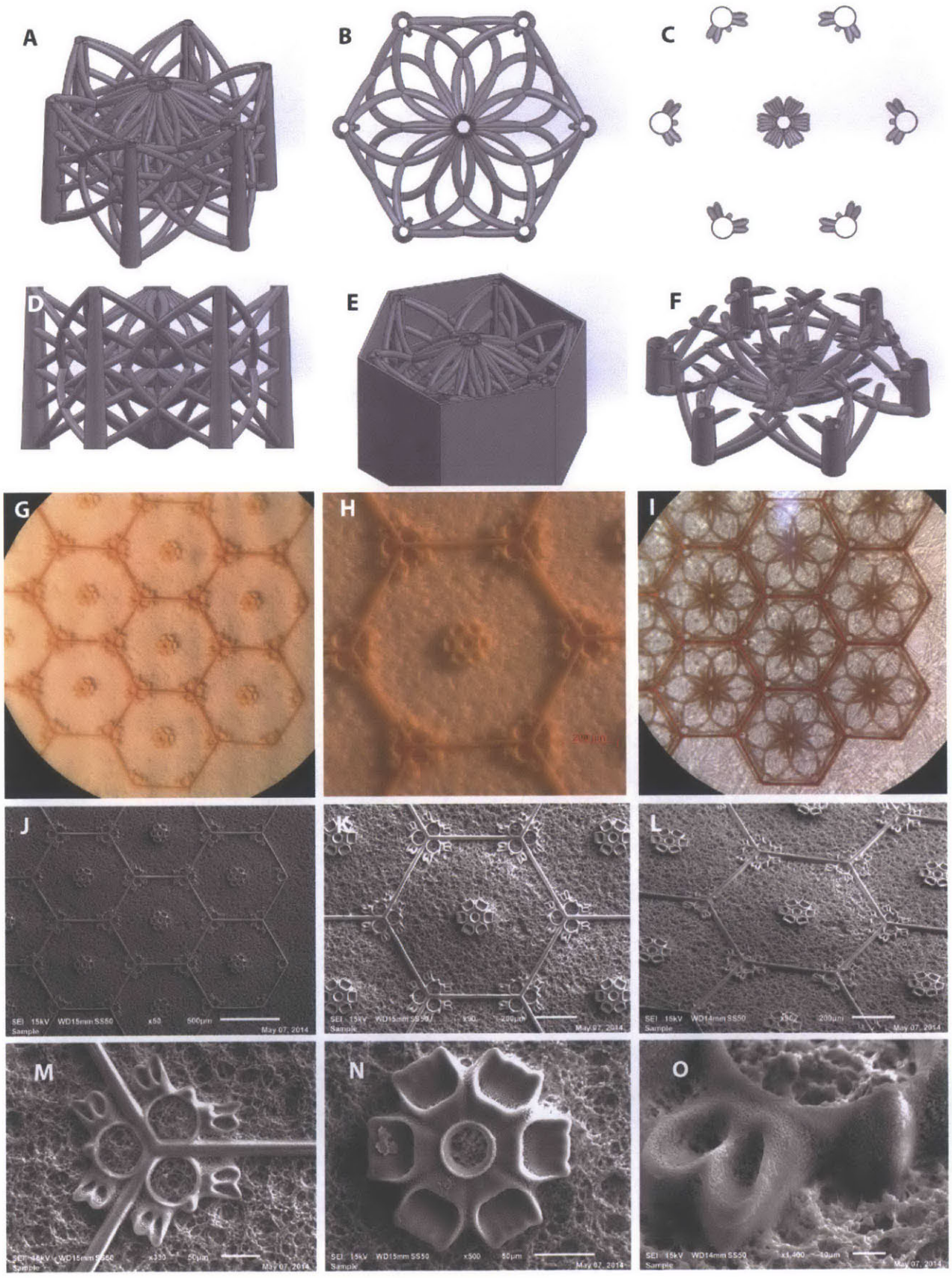
A
B
C
D
E
F
G
H
I
J
K
L
M
N
O

Conclusion and future work

The investigations discussed here provide a strong foundation for future research and biological testing. Fabrication protocols have been developed to make a broad range of scaffolds, complete with reliable codes, manual techniques, and a large library of design-specific resins. The final goal of this project will be to successfully minimize resolution to achieve fully free-form fabrication with no Z-bias, thereby allowing the biological testing of multiple scaffold types with varying degrees of vascularity. Because of the interplay among many fabrication variables, and because of the intimate effect three-dimensional design can have on the efficacy of a given parameter set, perfecting scaffold designs and fabrication protocols will require careful observation and CAD models drawn with multiple sets of variables in mind.

Conclusion

This project had three primary goals. First, a PuSL had to be fabricated that would allow the generation of three-dimensional complex acellular scaffolds across multiple length scales. Second, a resin set had to be developed that would allow the construction of scaffolds with macroscopic, microscopic, and nano-scale feature sizes. And third, a methodology had to be developed for visualizing, designing, and eventually fabricating scaffolds with complex microarchitecture.

The first aim has been successfully completed, and little work remains to validate the PuSL system. A working resin set has been engineered toward completion of the second aim, though research still remains to investigate and optimize the degradation rate of the cured material. Regarding the third aim, an extensive set of drafting, programming, and fabrication techniques has been developed toward the construction of a wide variety of scaffold designs. Ultimately, the work presented here comprises a functional toolset that might be used and mastered during the coming years.

PuSL has the potential to be a powerful tool for biomedical and tissue engineers because of its ability to fabricate almost any shape. For this same reason, the "best" scaffold type may not be determined for some time; since there are minimal fabrication constraints, optimization will have to come from biological testing. Biological input will become increasingly important for future work, as subtle architectural differences between scaffolds may have significant effect on cell growth and organization. Applied in the right fashion, PuSL has the potential to support a new paradigm in three-dimensional biological culture and experimentation, as it might allow the generation of tissues largely freed from mass-transport demands.

One of the primary questions at this point is what degree of scaffold vascularity is necessary, or preferred, for the generation of complex tissues. Although the ability to create near-capillary scale patent tubes is appealing, equally interesting is the possibility of generating spatial environments that keep large tissues alive while encouraging cell-directed vasculogenesis. The ultimate aim is a living, vascularized, macroscopic tissue, and this might be created in a variety of ways. Future research should focus on finding the most reliable and functional way of using PuSL to achieve this aim.

A surprisingly impactful constraint on the research described here has been the absorption of photoabsorber into the PDMS top plate. A priority is to reduce the cure-depth to single micron levels, and to do so may require finding alternate photoabsorbers or modifying the surface of the PDMS. The PuSL technique can be made truly free-form if the effective voxel size of the apparatus approaches ~1-3um^3. Once the current Z-direction cure bias is corrected, there will be few constraints in the CAD design space, and the tools will be in hand to generate rapidly almost any design, assuming it has been optimized for point-spread and thresholding effects.

The research presented here shows that we are close to generating functional scaffolds that display a biomimetic hierarchy of scale. A resin set has been found that locally cures to form a biocompatible, degradable nanoporous solid. Multiple scaffold designs have been drafted that display various degrees of histological organization. Bringing these two components together through the PuSL apparatus, we have the technology to pattern these scaffolds over broad, macroscopic areas with great precision. The next step is to complete rigorously controlled biological testing that will illuminate the best path for in vitro generation of complex tissues. By seeding the PuSL-fabricated constructs with cells and determining the right bioreactor culture

conditions, we could have the tools in hand to construct tissues in the laboratory that closely resemble those found in vivo.

References

1 Gupta, K. *et al.* Lab-on-a-chip devices as an emerging platform for stem cell biology. *Lab on a chip* **10**, 2019-2031 (2010).

2 Ota, H. *et al.* Three-dimensional spheroid-forming lab-on-a-chip using micro-rotational flow. *Sensors and Actuators B: Chemical* **147**, 359-365, doi:10.1016/j.snb.2009.11.061 (2010).

3 Zhang, C., Zhao, Z., Abdul Rahim, N. A., van Noort, D. & Yu, H. Towards a human-on-chip: culturing multiple cell types on a chip with compartmentalized microenvironments. *Lab on a chip* **9**, 3185-3192, doi:10.1039/b915147h (2009).

4 Bellan, L. M. *et al.* Fabrication of an artificial 3-dimensional vascular network using sacrificial sugar structures. *Soft Matter* **5**, 1354, doi:10.1039/b819905a (2009).

5 Wu, W., DeConinck, A. & Lewis, J. A. Omnidirectional printing of 3D microvascular networks. *Advanced materials* **23**, H178-183, doi:10.1002/adma.201004625 (2011).

6 Miller, J. S. *et al.* Rapid casting of patterned vascular networks for perfusable engineered three-dimensional tissues. *Nature materials* **11**, 768-774, doi:10.1038/nmat3357 (2012).

7 Huang, J.-H. *et al.* Rapid Fabrication of Bio-inspired 3D Microfluidic Vascular Networks. *Advanced materials* **21**, 3567-3571, doi:10.1002/adma.200900584 (2009).

8 Norotte, C., Marga, F. S., Niklason, L. E. & Forgacs, G. Scaffold-free vascular tissue engineering using bioprinting. *Biomaterials* **30**, 5910-5917, doi:10.1016/j.biomaterials.2009.06.034 (2009).

9 Domansky, K. *et al.* Perfused multiwell plate for 3D liver tissue engineering. *Lab on a chip* **10**, 51-58, doi:10.1039/b913221j (2010).

10 Griffith, L. G. & Swartz, M. A. Capturing complex 3D tissue physiology in vitro. *Nature reviews. Molecular cell biology* **7**, 211-224, doi:10.1038/nrm1858 (2006).

11 Tilles, A. W., Baskaran, H., Roy, P., Yarmush, M. L. & Toner, M. Effects of oxygenation and flow on the viability and function of rat hepatocytes cocultured in a microchannel flat-plate bioreactor. *Biotechnology and bioengineering* **73**, 379-389 (2001).

12 Griffith, L. G. *et al.* In Vitro Organogenesis of Liver Tissue. *Annals of the New York Academy of Sciences* **831**, 382-397 (1997).

13 Ohshima, N., Yanagi, K. & Miyoshi, H. Packed-Bed Type Reactor to Attain High Density Culture of Hepatocytes for Use as a Bioartificial Liver. *Artificial organs* **21**, 1169-1176 (1997).

14 Zeilinger, K. *et al.* Scaling down of a clinical three-dimensional perfusion multicompartment hollow fiber liver bioreactor developed for extracorporeal liver support to an analytical scale device useful for hepatic pharmacological in vitro studies. *Tissue engineering. Part C, Methods* **17**, 549-556, doi:10.1089/ten.TEC.2010.0580 (2011).

15 Itoga, K., Yamato, M., Kobayashi, J., Kikuchi, A. & Okano, T. Cell micropatterning using photopolymerization with a liquid crystal device commercial projector. *Biomaterials* **25**, 2047-2053, doi:10.1016/j.biomaterials.2003.08.052 (2004).

16 Lu, Y., Mapili, G., Suhali, G., Chen, S. & Roy, K. A digital micro-mirror device-based system for the microfabrication of complex, spatially patterned tissue engineering scaffolds. *Journal of biomedical materials research. Part A* **77**, 396-405, doi:10.1002/jbm.a.30601 (2006).

17 Leigh, S. J. *et al.* Fabrication of 3-dimensional cellular constructs via microstereolithography using a simple, three-component, poly(ethylene glycol) acrylate-based system. *Biomacromolecules* **14**, 186-192, doi:10.1021/bm3015736 (2013).

18 Choi, J.-W. *et al.* Fabrication of 3D biocompatible/biodegradable micro-scaffolds using dynamic mask projection microstereolithography. *Journal of Materials Processing Technology* **209**, 5494-5503, doi:10.1016/j.jmatprotec.2009.05.004 (2009).
19 Itoga, K., Kobayashi, J., Yamato, M., Kikuchi, A. & Okano, T. Maskless liquid-crystal-display projection photolithography for improved design flexibility of cellular micropatterns. *Biomaterials* **27**, 3005-3009, doi:10.1016/j.biomaterials.2005.12.023 (2006).
20 Melchels, F. P. *et al.* Mathematically defined tissue engineering scaffold architectures prepared by stereolithography. *Biomaterials* **31**, 6909-6916, doi:10.1016/j.biomaterials.2010.05.068 (2010).
21 Choi, J.-W., MacDonald, E. & Wicker, R. Multi-material microstereolithography. *The International Journal of Advanced Manufacturing Technology* **49**, 543-551, doi:10.1007/s00170-009-2434-8 (2009).
22 Billiet, T., Vandenhaute, M., Schelfhout, J., Van Vlierberghe, S. & Dubruel, P. A review of trends and limitations in hydrogel-rapid prototyping for tissue engineering. *Biomaterials* **33**, 6020-6041, doi:10.1016/j.biomaterials.2012.04.050 (2012).
23 Melchels, F. P., Feijen, J. & Grijpma, D. W. A review on stereolithography and its applications in biomedical engineering. *Biomaterials* **31**, 6121-6130, doi:10.1016/j.biomaterials.2010.04.050 (2010).
24 Sun, C., Fang, N., Wu, D. M. & Zhang, X. Projection micro-stereolithography using digital micro-mirror dynamic mask. *Sensors and Actuators A: Physical* **121**, 113-120, doi:10.1016/j.sna.2004.12.011 (2005).
25 Xia, C. & Fang, N. X. 3D microfabricated bioreactor with capillaries. *Biomedical microdevices* **11**, 1309-1315, doi:10.1007/s10544-009-9350-4 (2009).
26 Toshima, M., Ohtani, Y. & Ohtani, O. Three-dimensional architecture of elastin and collagen fiber networks in the human and rat lung. *Archives of histology and cytology* **67**, 31 (2004).
27 Kim, B. S. *et al.* Facile preparation of biodegradable glycol chitosan hydrogels using divinyladipate as a crosslinker. *Macromolecular Research* **17**, 734-738 (2009).
28 Dai, S., Xue, L., Zinn, M. & Li, Z. Enzyme-Catalyzed Polycondensation of Polyester Macrodiols with Divinyl Adipate: A Green Method for the Preparation of Thermoplastic Block Copolyesters. *Biomacromolecules* **10**, 3176-3181, doi:10.1021/bm9011634 (2009).
29 Hiraguri, Y., Katase, K. & Tokiwa, Y. Synthesis of Biodegradable Hydrogel by Radical Ring-Opening Polymerization of 2-Methylene-1,3,6-Trioxocane. *Journal of Macromolecular Science, Part A* **43**, 1021-1027, doi:10.1080/10601320600740033 (2006).
30 Husár, B. *et al.* Biomaterials based on low cytotoxic vinyl esters for bone replacement application. *Journal of Polymer Science Part A: Polymer Chemistry* **49**, 4927-4934, doi:10.1002/pola.24933 (2011).
31 Heller, C. *et al.* Vinyl esters: Low cytotoxicity monomers for the fabrication of biocompatible 3D scaffolds by lithography based additive manufacturing. *Journal of Polymer Science Part A: Polymer Chemistry* **47**, 6941-6954, doi:10.1002/pola.23734 (2009).
32 Heller, C. *et al.* Vinylcarbonates and vinylcarbamates: Biocompatible monomers for radical photopolymerization. *Journal of Polymer Science Part A: Polymer Chemistry* **49**, 650-661, doi:10.1002/pola.24476 (2011).
33 Zheng, X. *et al.* Design and optimization of a light-emitting diode projection micro-stereolithography three-dimensional manufacturing system. *Review of Scientific Instruments* **83**, 125001 (2012).

34 Chiu, L. L., Montgomery, M., Liang, Y., Liu, H. & Radisic, M. Perfusable branching microvessel bed for vascularization of engineered tissues. *Proceedings of the National Academy of Sciences* **109**, E3414-E3423 (2012).
35 Baiguera, S. & Ribatti, D. Endothelialization approaches for viable engineered tissues. *Angiogenesis* **16**, 1-14 (2013).

Acknowledgements

I would like to express my gratitude to my thesis co-advisors Linda Griffith, Paula Hammond, and Jeffrey Borenstein. This work would not have been possible without their support and guidance. It has been a privilege to work with them, and I am thankful for having been allowed the creative space to pursue this research.

I would also like to thank the Draper Laboratory Fellow Program, which has supported my education during the past two years. It has been an extraordinary opportunity to work between MIT and Draper Laboratories and to gather the tools and expertise to realize the vision described here.

I am deeply indebted to Nick Fang and Howon Lee, whose research laid the foundation for this thesis and who developed many of the PuSL techniques described within this document. Their expertise and advice were invaluable. This research would have been impossible without them.

I would like to thank Dave Brancazio for his help engineering the PuSL apparatus; Hsinhwa Lee for her never-ending support; Jonathan Coppetta, Dan Heath, Walker Inman, Kasper Renggli, and Jackie Shepard, for their help thinking through challenges; Caitlin Mackey and Keisuke Matsushita for their input and help, and the DMSE administration for helping everything to run smoothly.

Finally, I would like to thank my family and community for their patience and support. I especially need to thank my mother, Harriet Brickman, and my father, Thomas Raredon, for their guidance and insight.

This work was completed with funding from the National Institutes of Health and the Defense Advanced Research Projects Agency.